



Influence of vmPFC on dmPFC Predicts Valence-Guided Belief Formation

Kuzmanovic, Bojana ; Rigoux, Lionel ; Tittgemeyer, Marc

Abstract: When updating beliefs about their future prospects, people tend to disregard bad news. By combining fMRI with computational and dynamic causal modeling, we identified neurocircuitry mechanisms underlying this optimism bias to test for valence-guided belief formation. In each trial of the fMRI task, participants ($n = 24$, 10 male) estimated the base rate (eBR) and their risks of experiencing negative future events, were confronted with the actual BR, and finally had the opportunity to update their initial self-related risk estimate. We demonstrated an optimism bias by revealing greater belief updates in response to good over bad news (i.e., learning that the actual BR is lower or higher than expected) while controlling for confounds (estimation error and personal relevance of the new information). Updating was favorable when the final belief about risks improved (or at least did not worsen) relative to the initial risk estimate. This valence of updating was encoded by the ventromedial prefrontal cortex (vmPFC) associated with the valuation of rewards. Within the updating circuit, the vmPFC filtered the incoming signal in a valence-dependent manner and influenced the dorsomedial prefrontal cortex (dmPFC). Both the valence-encoding activity in the vmPFC and its influence on the dmPFC predicted individual magnitudes of the optimism bias. Our results indicate that updating was biased by the motivation to maximize desirable beliefs, mediated by the influence of the valuation system on further cognitive processing. Therefore, although it provides the very basis for human reasoning, belief formation is essentially distorted to promote desired conclusions. **SIGNIFICANCE STATEMENT** The question of whether human reasoning is biased by desires and goals is crucial for everyday social, professional, and economic decisions. How much our belief formation is influenced by what we want to believe is, however, still debated. Our study confirms that belief updates are indeed optimistically biased. Critically, the bias depends on the recruitment of the brain valuation system and the influence of this system on neural regions involved in reasoning. These neurocircuit interactions support the notion that the motivation to maximize pleasant beliefs reinforces those cognitive processes that are most likely to yield the desired conclusion.

DOI: <https://doi.org/10.1523/jneurosci.0266-18.2018>

Posted at the Zurich Open Repository and Archive, University of Zurich

ZORA URL: <https://doi.org/10.5167/uzh-158350>

Journal Article

Accepted Version

Originally published at:

Kuzmanovic, Bojana; Rigoux, Lionel; Tittgemeyer, Marc (2018). Influence of vmPFC on dmPFC Predicts Valence-Guided Belief Formation. *Journal of Neuroscience*, 38(37):7996-8010.

DOI: <https://doi.org/10.1523/jneurosci.0266-18.2018>

Research Articles: Behavioral/Cognitive

Influence of vmPFC on dmPFC Predicts Valence-Guided Belief Formation

Bojana Kuzmanovic¹, Lionel Rigoux^{1,2} and Marc Tittgemeyer¹

¹*Translational Neurocircuitry Group, Max Planck Institute for Metabolism Research Cologne, 50931 Cologne, Germany*

²*Translational Neuromodeling Unit (TNU), Institute for Biomedical Engineering, University of Zurich and ETH Zurich, 8032 Zurich, Switzerland*

DOI: 10.1523/JNEUROSCI.0266-18.2018

Received: 30 January 2018

Revised: 17 July 2018

Accepted: 20 July 2018

Published: 13 August 2018

Author contributions: B.K. designed research; B.K. performed research; B.K. and L.R. analyzed data; B.K. wrote the first draft of the paper; B.K., L.R., and M.T. edited the paper; B.K., L.R., and M.T. wrote the paper.

Conflict of Interest: The authors declare no competing financial interests.

We thank Morné Truter for proofreading and valuable comments on an earlier draft of the manuscript and Thorben Huelsduenker for assistance with data collection.

Corresponding Author: Bojana Kuzmanovic, Max Planck Institute for Metabolism Research, Translational Neurocircuitry Group, Gleuelerstr. 50, 50931 Cologne, Germany, Tel.: +49 221 4726-255, Email: bojana.kuzmanovic@sf.mpg.de

Cite as: J. Neurosci ; 10.1523/JNEUROSCI.0266-18.2018

Alerts: Sign up at www.jneurosci.org/cgi/alerts to receive customized email alerts when the fully formatted version of this article is published.

1 **Influence of vmPFC on dmPFC**
2 **Predicts Valence-Guided Belief Formation**

3
4 Abbreviated Title:
5 **Neurocircuits of Valence-Guided Belief Formation**

6
7 Bojana Kuzmanovic^{1*}, Lionel Rigoux^{1,2}, Marc Tittgemeyer¹

8 ¹ Translational Neurocircuitry Group, Max Planck Institute for Metabolism Research
9 Cologne, 50931 Cologne, Germany

10 ² Translational Neuromodeling Unit (TNU), Institute for Biomedical Engineering, University
11 of Zurich and ETH Zurich, 8032 Zurich, Switzerland

12
13 * Corresponding Author:

14 Bojana Kuzmanovic
15 Max Planck Institute for Metabolism Research
16 Translational Neurocircuitry Group
17 Gleuelerstr. 50, 50931 Cologne, Germany
18 Tel.: +49 221 4726-255
19 Email: bojana.kuzmanovic@sf.mpg.de

20
21 Number of pages: 51; Number of figures: 4; Number of tables: 4.

22 Number of words: Abstract 248, Introduction 644, and Discussion 1500.

23
24 Conflict of Interest: The authors declare no competing financial interests.

25 Acknowledgments: We thank Morné Truter for proofreading and valuable comments on an
26 earlier draft of the manuscript and Thorben Huelsduenker for assistance with data collection.

27 **Abstract**

28

29 When updating beliefs about their future prospects, people tend to disregard bad news.

30 By combining fMRI with computational and dynamic causal modeling, we identified

31 neurocircuitry mechanisms underlying this optimism bias to test for valence-guided belief

32 formation. In each trial of the fMRI task, participants ($n = 24$, 10 male) estimated the base rate

33 and their risks of experiencing negative future events, were confronted with the actual base

34 rate, and finally had the opportunity to update their initial self-related risk estimate. We

35 demonstrated an optimism bias by revealing greater belief updates in response to good over

36 bad news (i.e., learning that the actual base rate is *lower* or *higher* than expected), while

37 controlling for confounds (estimation error and personal relevance of the new information).

38 Updating was favorable when the final belief about risks *improved* (or at least did not

39 worsened) relative to the initial risk estimate. This valence of updating was encoded by the

40 ventromedial prefrontal cortex (vmPFC) associated with the valuation of rewards. Within the

41 updating circuit, the vmPFC filtered the incoming signal in a valence-dependent manner and

42 influenced the dorsomedial prefrontal cortex (dmPFC). Both the valence-encoding activity in

43 the vmPFC and its influence on the dmPFC predicted individual magnitudes of the optimism

44 bias. Our results indicate that updating was biased by the motivation to maximize desirable

45 beliefs, mediated by the influence of the valuation system on further cognitive processing.

46 Thus, while providing the very basis for human reasoning, belief formation is essentially

47 distorted to promote desired conclusions.

48 **Significance Statement**

49

50 The question whether human reasoning is biased by desires and goals is crucial for everyday
51 social, professional, and economic decisions. How much our belief formation is influenced by
52 what we *want* to believe is, however, still debated. Our study confirms that belief updates are
53 indeed optimistically biased. Critically, the bias depends on the recruitment of the brain
54 valuation system and the influence of this system on neural regions involved in reasoning.
55 These neurocircuit interactions support the notion that the motivation to maximize pleasant
56 beliefs reinforces those cognitive processes that are most likely to yield the desired
57 conclusion.

Introduction

Not only extrinsic rewards such as tasty food, but also internal processes such as desirable beliefs or positive emotions are expected to evoke pleasant states. Believing that one is attractive and intelligent (Eil and Rao, 2011; Korn et al., 2012), or that one's future will be bright (Sharot et al., 2011), has a positive subjective value, which is why people tend to be motivated to maintain such beliefs (Sharot and Garrett, 2016a). In turn, the motivation to maximize pleasant beliefs has been hypothesized to reinforce those cognitive processes that are most likely to yield a desired conclusion (Kunda, 1990; Hughes and Zaki, 2015).

However, motivational influences on reasoning have been controversially debated (Kunda, 1990; Shah et al., 2016; Sharot and Garrett, 2016b; Kuzmanovic and Rigoux, 2017). But how can we prove whether specific conclusions are reinforced by desires when these processes are hidden from direct observation and can operate outside of awareness (Tesser, 2000)? One way is to identify systematic, valence-dependent biases in information integration. For instance, when participants were given new information relevant to their current belief, they were more likely to incorporate good than bad news (e.g., indicating a *lower* versus *higher* risk than initially expected) to update their belief (Sharot et al., 2011; Kuzmanovic et al., 2016a). Circumventing self-report, such asymmetric updating provides an individual index of the optimism bias by exploiting actual belief formation behavior.

Another difficulty is that no reward has a fix subjective value, neither the extrinsic nor the intrinsic ones. Tasty food, for instance, is more pleasant during a hungry state. This is directly reflected in the activity of brain regions encoding the reward value such as the ventromedial prefrontal cortex (vmPFC; Bartra et al., 2013; Chase et al., 2015): neurons in the vmPFC that fired in response to tasty food during a hungry state, no longer showed this response after satiety (Grabenhorst and Rolls, 2011). Likewise, desirable beliefs may be more pleasant after threatening a person's self-worth (Roese and Olson, 2007; Rudman et al.,

2007). Indeed, the magnitude of the optimism bias substantially varied across the participants (e.g., Sharot et al., 2011; Kuzmanovic and Rigoux, 2017). We assume that the belief updating should be biased only in the subjects who indeed assign a positive value to avoiding threatening and enhancing desirable beliefs. This allows us to infer the current value of a specific reward (favorable beliefs) from the reinforcement of the behavior leading to this reward (updating biased towards favorable beliefs).

The present study aims to demonstrate that desirable beliefs have an incentive salience and therefore can guide updates by influencing ongoing cognitive processing. To this end, neural circuits of belief updating were identified by using an established fMRI paradigm. Recently (Kuzmanovic et al., 2016a), we have shown that the vmPFC encoded the positive value of favorable self-related (but not other-related) belief updates, indicating that the brain transforms beliefs into the same common value scale as classical rewards. Further, we isolated cognitive components and formally controlled for confounds using computational modeling to validate conclusions about valence-dependent update behavior (Kuzmanovic and Rigoux, 2017). Based on this previous work and the central role of the vmPFC in value encoding (Bartra et al., 2013; Chase et al., 2015), we hypothesized that the positive value of favorable updating would be encoded by the vmPFC. Moreover, we expected that only those individuals, who showed an optimism bias, will have a strong neural response to favorable updating. Finally, we used dynamic causal modeling to investigate mechanisms underlying valence-dependent updating. We hypothesized that the contexts of favorable and unfavorable updating would modulate coupling amongst regions recruited during updating, and that the identified valuation system would influence other regions involved in belief formation. Our results provide evidence for a motivationally biased belief formation that is mediated by the value encoding in the vmPFC, and the influence of the vmPFC on the dorsomedial prefrontal cortex.

109 **Materials and Methods**

110

111 *Participants*

112

113 Forty subjects were recruited from the institute's subject database. A total of four
 114 participants was excluded because of problems with task performance. Two participants
 115 recognized that the base rates were manipulated, and one individual did not update estimates
 116 in 84% of trials (mean of the included sample = 30.09%, $SD = 16.13$; exclusion threshold =
 117 66.67%). Lastly, one participant updated estimates away from the presented base rate in 18%
 118 of trials indicating problems with task understanding (mean of the included sample = 2.66%,
 119 $SD = 4.12$; exclusion threshold = 15%). Data from another 12 participants were excluded due
 120 to excessive head movement in the MR scanner that exceeded a threshold of 1.5 framewise
 121 displacement (Power et al., 2012). This was necessary to account for increased sensitivity to
 122 motion-related artifacts in multiband acquisition for functional imaging (see below for
 123 acquisition parameters). Thus, in total 24 subjects were included into the analysis (10 male,
 124 mean age = 27.38, $SD = 5.15$). Notably, adding the 12 subjects with excessive motion to the
 125 sample of 24 subjects revealed the same behavioral results (see Results, Task Performance).

126

127 *Experimental Design*

128

129 The experiment was conducted during the acquisition of fMRI scans using Presenta-
 130 tion 18.1 (Neurobehavioral Systems) and consisted of 80 trials with 80 different adverse life
 131 events (e.g., cancer or car theft). Participants began each trial with estimating the base rate of
 132 an adverse life event (eBR, see **Figure 1**). Next, they were asked to estimate their own likeli-
 133 hood of experiencing the life event in their lifetime (first estimate, E1), and were subsequently
 134 presented with the actual base rate (BR). Subjects were instructed that the base rate refers to

135 the probability of the respective event occurring to persons of the same sex and age, living in
 136 the same socio-cultural environment, as determined by the German Federal Statistical Office
 137 (“Statistisches Bundesamt”). At the end of each trial, participants had to re-estimate their own
 138 risk (second estimate, E2).

139 The critical behavioral measure was the size of the update, i.e., the difference between
 140 E1 and E2. Subjects were expected to update their first risk estimate after being confronted
 141 with a base rate different than the one they initially assumed. This difference between eBR
 142 and BR indicated the estimation error (EE; $EE = |eBR - BR|$). In half of the trials, BR was de-
 143 sirable (better than expected, i.e., $eBR > BR$; good news, GOOD), and in the other half, BR
 144 was undesirable (worse than expected, i.e., $eBR < BR$; bad news, BAD). Notably, we ex-
 145 pected participants to change their risk estimates on average toward the new information. That
 146 is, upon an actual base rate that is lower than expected, participants should decrease their risk
 147 estimates. Conversely, upon an actual base rate that is higher than expected, participants
 148 should increase their risk estimates. Indeed, updates toward the direction opposed to the new
 149 information were very rare ($M = 2.66\%$, $SD = 4.12$). This is also reflected in the desirability-
 150 dependent computation of updates that ensures that positive values indicate an update toward
 151 the new information equally for GOOD and BAD (see Table 1). Valence-dependent bias in
 152 updating was present when GOOD and BAD trials yielded different updates (i.e., mean updat-
 153 e_{GOOD} > mean update_{BAD} indicates an optimism bias).

154 Participants were free to report a probability anywhere between 1 and 99%. Starting
 155 from 50% in eBR, they selected the desired probability by using two buttons to increase or de-
 156 crease the number displayed on the screen (**Figure 1**, green font in eBR, E1, and E2), and a
 157 third button to confirm the selected choice. Subjects were instructed to use both hands. In the
 158 first half of the experiment they used the right hand for selecting the percentage number and

the left hand for confirming it, and in the second half the other way around (order counter-balanced across subjects). In E1, the starting number equaled the one selected in eBR, and in E2, the starting number corresponded to the one selected in E1.

For eBR, E1, and E2, the response display was activated after a 2 s interval. Subjects were instructed to use the first 2 s to think about their estimate, and then had a maximum of 10 s to respond (see **Table 1** for mean RTs). BR was presented for 2 s. The intervals within and between the trials consisted of a fixation cross and were jittered (Mumford et al., 2015): the three inter-stimulus intervals within the trial (between eBR and E1, E1 and BR, and BR and E2) ranged between 2375 ms and 4625 ms, with a mean of 3500 ms, and the inter-trial intervals ranged between 4875 ms and 7125 ms, with a mean of 6000 ms. The average task duration was 48 min ($SD = 2.45$).

GOOD and BAD trials were rendered comparable with respect to i) number of trials, ii) mean size of estimation error, and iii) range of actual base rates (BR). Furthermore, the assignment of stimuli to the two conditions (GOOD and BAD), the different estimation error sizes, and the order of trials were randomized anew for each subject. This was accomplished by manipulating the BR, unbeknownst to subjects. To generate a desirable BR, a number between 1 and 25 was subtracted from the estimated BR (eBR), and to generate an undesirable BR, a number between 1 and 25 was added to the eBR. In addition, BRs were capped between 1 and 90% because base rates exceeding this range are likely to appear implausible.

However, this manipulation of BR was sometimes constrained by subjects' responses. For instance, when the eBR was close to or greater than 90%, trials that were scheduled to generate bad news could not be realized (e.g., when eBR was 90%, no greater BR could be generated because BRs were capped between 1% and 90%). Instead, a number lower than 90% was presented (a random number between 85% and 90%), generating good news. This reversal of the scheduled trial valence ($M = 1.30$, $SD = 2.20$) can be made responsible for the

185 condition-wise differences in number of trials (the reversal occurred only in BAD trials,
 186 thereby decreasing the number of realized BAD trials and increasing the number of realized
 187 GOOD trials), and eBR and E1 (only BAD trials with high eBRs were possible candidates for
 188 such a reversal, and eBR and E1 were highly correlated, as one would expect, see **Figure 2E-**
 189 **F**). Supporting this assumption, number of trials and eBR differed between the conditions
 190 only in subjects with reversals (and/or EE = 0; $t(11) = 2.68, p = .022$, eBR, $t(11) = 6.86, p <$
 191 $.001$), but not in subjects without such irregularities ($t(11) = 0.32, p = .755$, eBR, $t(11) = 2.06,$
 192 $p = .064$). Notably, we nevertheless achieved satisfactory balanced distributions of number of
 193 trials, eBR, E1, and EE between conditions (e.g., on average 78.17 of 80 trials could be
 194 realized, and the mean difference between GOOD and BAD was 1.75 trials; see Table 1).
 195 Additional details on the experimental design and the BR manipulation algorithm have been
 196 described elsewhere (Kuzmanovic and Rigoux, 2017).

197 Before the experiment, all participants received written instructions, and completed six
 198 practice trials with stimulus events not used in the experiment. In a final debriefing after the
 199 experiment, a funneled procedure was used to ensure that subjects did not suspect the
 200 manipulation of the base rates, or the purpose of the study. All procedures were in accordance
 201 with the World Medical Association Declaration of Helsinki and were approved by the local
 202 ethics committee of the Medical Faculty of the University of Cologne, Germany (15-255).

203
 204 *Acquisition parameters.* The MRI data were acquired by using a Magnetom Trio
 205 Prisma^{fit} 3T whole body scanner and a 64-channel head coil (Siemens AG, Medical Solutions,
 206 Erlangen, Germany). During the update experiment, fMRI data were acquired in one session
 207 with a slice accelerated multiband echo planar imaging sequence (Xu et al., 2013) covering
 208 the whole brain (TR = 1050 ms, TE = 37.40 ms, field of view = $212 \times 212 \times 144 \text{ mm}^3$, voxel
 209 size = $2 \times 2 \times 2 \text{ mm}^3$, 72 oblique axial slices, multiband acceleration factor 6). In addition, we
 210 acquired two images with reversed phase encoding directions (anterior-posterior or posterior-

211 anterior) for the purpose of estimating and correcting the susceptibility-induced distortion
 212 using topup (TR 8240 ms, TE 69 ms, field of view $212 \times 212 \times 144 \text{ mm}^3$, voxel size $2 \times 2 \times 2$
 213 mm^3 , 72 oblique axial slices). High-resolution T1-weighted images were obtained from the
 214 institute's subject database (MDEFT, TR 1930 ms, TE 5.80 ms, field of view $256 \times 256 \times 160$
 215 mm^3 , voxel size $1 \times 1 \times 1.25 \text{ mm}^3$, 128 sagittal slices, or MPRAGE, TR 2300 ms, TE 2.32
 216 ms, field of view $256 \times 256 \times 192 \text{ mm}^3$, voxel size $0.9 \times 0.9 \times 0.9 \text{ mm}^3$, 213 sagittal slices).

217

218 *Statistical Analyses*

219

220 *Analysis of Task Performance*

221

222 Prior to analyses, the following trials were excluded: trials with missing responses (M
 223 $= 0.83$, $SD = 1.01$), trials with $EE = 0$ (e.g., when eBR was 1% in a GOOD trial, BR was also
 224 1%; $M = 0.88$, $SD = 1.26$), and outliers (trials in which the update exceeded 4 SD of the
 225 subjects' mean; $M = 0.13$, $SD = 0.34$). For each subject, trials were divided into two
 226 conditions: *good news* (GOOD; $BR < eBR$) and *bad news* (BAD; $BR > eBR$). Optimism bias
 227 was assessed by comparing updates in GOOD-trials with those in BAD-trials (mean
 228 $\text{update}_{\text{GOOD}} - \text{mean update}_{\text{BAD}}$). Note that on average participants were expected to decrease
 229 their risk estimates after good news and to increase their risk estimates after bad news. Thus,
 230 for both $\text{update}_{\text{GOOD}}$ and $\text{update}_{\text{BAD}}$, positive values indicate an update towards the new
 231 information (see **Table 1** for statistics of task variables; also see **Figure 2A**). Furthermore, for
 232 each participant, we conducted a linear regression to predict his or her updates on each trial
 233 using valence of news (GOOD vs. BAD), while including eBR, E1, and EE as covariates (all
 234 measures z-scored within subject). For repeated measures, the standard deviation of the paired
 235 differences was used as a standardizer for Cohen's d (Cumming, 2014).

236 In addition, we performed computational modeling of belief updating. The model-
 237 based approach allows to formally control for fluctuations in trial-wise eBR, E1, and EE
 238 across conditions, and to simulate unbiased updating based on observed trial-wise EE and
 239 personal relevance (PR). Building on previous work (Kuzmanovic and Rigoux, 2017), the
 240 model of belief updating was formalized as follows:

241

$$242 \quad \text{Update} = LR * EE * PR$$

$$243 \quad \text{With } LR_{GOOD} = Alpha + Asymmetry$$

$$244 \quad LR_{BAD} = Alpha - Asymmetry$$

245

246 This model relies on the generic form of reinforcement learning, in which update is
 247 proportional to the *estimation error* EE (equivalent to prediction error). In addition, EE is
 248 weighted by the *learning rate* (LR), which indicates the general tendency of each subject to
 249 update their beliefs in response to the EE. In order to test for the optimism bias (asymmetric
 250 learning), LR was estimated separately for good and bad news (see also Palminteri et al.,
 251 2016; Lefebvre et al., 2017) and therefore has two components. The general component,
 252 *Alpha* (α), indicates the tendency to learn from errors, independent of the valence of news.
 253 *Alpha* equal 1 indicates that update is exactly equal to EE, while α smaller than 1 indicates
 254 updates smaller than EE. *Asymmetry* (A) equal zero indicates equal learning rates for GOOD
 255 and BAD, while A different from zero indicates that the resulting learning rates systematically
 256 differ for GOOD and BAD (e.g., *Asymmetry* > zero indicates lower learning rates and hence
 257 smaller updates for BAD than for GOOD).

258 EE is also weighted by the *personal relevance* (PR; corresponds to ‘relative personal
 259 knowledge’ in Kuzmanovic and Rigoux, 2017). PR indicates the difference between eBR and
 260 E1 relative to the maximal possible difference in each trial (see **Table 1** for the exact
 261 equation). Recently, we have demonstrated that the computational model of belief updating

262 that weighted EE with PR was superior to the model without any consideration of PR
 263 (Kuzmanovic and Rigoux, 2017). This shows that the more people felt detached from the
 264 reference population, the more irrelevant base rates became for their updates of risk estimates
 265 (e.g., if I do not have a car, I will not consider the base rate of car theft). PR ranged from 0 to
 266 1, with $PR = 1$ when a subject perceives her risk to be equal to those of the average person
 267 ($eBR = E1$, see **Figure 1** for an example), and $PR = 0$ when the perceived difference (eBR vs.
 268 $E1$) is maximal. Thus, EE weighted by PR indicates a subjective error (SE), where the impact
 269 of the EE on update is also determined by the personal relevance of the new information.

270 Using the VBA toolbox (Daunizeau et al., 2014), we implemented competing models
 271 and tested which of these best accounted for the observed update behavior. In order to test
 272 whether *Alpha* was different from 1 and whether *Asymmetry* was different from 0, we
 273 generated all possible variations of the update equation by switching the parameters *Alpha*
 274 and *Asymmetry* on (by letting the parameter free), or off (by fixing the parameter's prior
 275 variance to zero). Thus, 4 models (αA , α , A , \emptyset ; α and A indicate that the respective parameter
 276 was let free) were estimated for each subject. Note that by setting *Asymmetry* to 0 (i.e.,
 277 models α and \emptyset) we specified the null hypothesis that learning is unbiased. In the alternative
 278 hypothesis (i.e., models αA and A), *Asymmetry* was estimated for each participant. Model
 279 estimations yielded a posterior distribution across the parameters, and an approximation to the
 280 evidence of the model. The approximated model evidence reflects the goodness of fit,
 281 penalized for the complexity. We used the Free-energy approximation that has been shown to
 282 be superior to other approximations like AIC or BIC (Penny, 2012). Model evidences of all
 283 subjects and all tested models were then entered in a random-effect Bayesian model
 284 comparison. For each model, this procedure estimates a) the probability of each subject to be
 285 best described by the respective model (model attributions), b) the frequency in the population
 286 (estimated model frequency, Ef), and c) the protected exceedance probability (pxp), which is

287 the probability that the model predominates in the population, above and beyond chance (see
 288 Rigoux et al., 2014 for more details).

289

290 *fMRI Analyses*

291

292 Prior to analysis, the first ten volumes were discarded to allow for magnetic saturation.

293 First, functional images were corrected for motion and distortion using the FSL (version
 294 5.0.9) tools MCFLIRT and topup (Andersson et al., 2003; Smith et al., 2004). All further
 295 analysis steps including DCM were conducted using SPM12 (Wellcome Trust Centre for
 296 Neuroimaging, London, UK) implemented in MATLAB R2014b (The Mathworks Inc.,
 297 Massachusetts, USA). The T1 image was normalized to the Montreal Neurological Institute
 298 (MNI) reference space using the unified segmentation approach, and the ensuing deformation
 299 parameters were applied to (previously coregistered) functional images. Finally, functional
 300 images were smoothed using an 8 full-width-half-maximum Gaussian kernel.

301 Statistical analyses were conducted in the framework of a general linear model
 302 (GLM). At the single-subject level, conditions were modeled using a boxcar reference vector
 303 convolved with the canonical hemodynamic response function and its time derivative.
 304 Following events were modeled on separate regressors: eBR, E1, BR, E2, responses and rest.
 305 The duration of eBR, E1, BR, and E2 was always set to 2 s, as for events with responses (all
 306 except of BR) the response display was activated only after 2 s. Responses for all events were
 307 modeled on one regressor (duration from the onset of the response event to the confirmation
 308 button press, which was also the beginning of the next inter-stimulus-interval). The
 309 instruction to switch hands after the first half of trials, and the excluded trials (missing
 310 responses, $EE = 0$, and outliers; see *Analysis of Task Performance*), if present, were modeled
 311 on the ‘rest’ regressor. Motion parameters and a matrix with motion-outlier volumes
 312 (identified using the tool `fsl_motion_outlier` at a threshold of 4 *SD* of intensity differences

313 between subsequent volumes (Power et al., 2012)) were included as multiple regressors of no
 314 interest. Low-frequency signal drifts were filtered using a cutoff of 128 s. At the group-level,
 315 flexible factorial design and a significance threshold of $p < .05$, FWE-corrected at the peak
 316 level, with an extent threshold of 20 voxels were used. For the covariate analyses, we applied
 317 the same statistical threshold, but a lower extent threshold of 10 voxels.

318
 319 *Error Tracking.* We identified brain regions that encoded the errors experienced
 320 during the BR event. At that time, subjects were confronted with a different actual base rate
 321 than the one they have estimated (i.e., the difference between eBR and BR). In order to obtain
 322 the effects separately for GOOD and BAD, we split the BR trials into BR_{GOOD} and BR_{BAD},
 323 and tested for parametric modulation (PM) by subjective error ($SE = EE * PR$, see *Analysis of*
 324 *Task Performance*). We focused on this subjective error processing because it was more
 325 relevant for the subsequent belief updating than the general error (i.e., EE; Kuzmanovic and
 326 Rigoux, 2017). The resulting 9 regressors (eBR, E1, BR_{GOOD}, PM_error_{GOOD}, BR_{BAD},
 327 PM_error_{BAD}, E2, responses, and rest) were only weakly correlated (\bar{r} s, averaged across
 328 subjects, between -.29 and .14), indicating efficient parameter estimation. At the single-
 329 subject level, two contrast images were computed relative to the implicit baseline
 330 (PM_error_{GOOD} and PM_error_{BAD}) and entered into group-level analysis. At the group level,
 331 we identified those regions that exhibited increasing or decreasing activation with increasing
 332 subjective error in both GOOD and BAD trials (global conjunction). Furthermore, we
 333 explored differences between PM_error_{GOOD} and PM_error_{BAD} and reported global
 334 conjunction results for significant results to clarify whether the difference related to different
 335 magnitudes of the same modulation effect (e.g., the positive correlation between BOLD and
 336 error was stronger in BAD than in GOOD), or to modulation effects of opposite direction
 337 (e.g., the correlation between BOLD and error was positive in BAD, but negative in GOOD).
 338 In order to be able to illustrate group effects of different sizes of error on the BOLD signal,

we also computed a GLM that models three sizes of error (small, mid and large) on 3 separate regressors, separately for GOOD and BAD (**Figure 3A**, line chart). ‘Small’, ‘mid’, and ‘large’ categories were generated by dividing the sorted array of values into three subarrays that i) do not share same values, and ii) are maximally similar with respect to the number of elements (this procedure was the same for errors and update’, see below). Finally, we tested whether the extent of error tracking correlated with the learning rate component *Alpha* across subjects by conducting a covariate analysis with one contrast per subject (average effect of PM_errorGOOD and PM_errorBAD).

The Valence of Updating. In order to identify brain regions that encoded the valence of updating, we focused on the E2 event because at that time subjects were deciding upon updating their initial belief. E2 trials were split into E2GOOD and E2BAD trials so that effects can be examined separately for GOOD and BAD. According to the valence of updating schematically shown in **Figure 3B** (gray box), we tested for the positive correlation between the BOLD-signal and update in GOOD trials, and for the negative correlation in BAD trials. To identify these opposed effects, we applied parametric modulation of E2GOOD and E2BAD, respectively, by update size. The advantage of the PM procedure is that it allows to adjust the effect of update for EE, PR, and other potential confounds (e.g., by including three orthogonalized parameters in the following order: PR, EE, update; Mumford et al., 2015). The resulting 13 regressors (eBR, E1, BR, E2GOOD, PM_PRGOOD, PM_EEGOOD, PM_updateGOOD, E2BAD, PM_PRBAD, PM_EEBAD, PM_updateBAD, responses, and rest) were only weakly correlated (\bar{r} s, averaged across subjects, between -.29 and .03), indicating efficient parameter estimation. The only exception was the negative correlation between BR and response ($\bar{r} = -.49$), which occurred because BR was the only event in the trial that was never associated with a subsequent motor response. Six contrast images were computed relative to the implicit baseline (PM_PR, PM_EE, and PM_update, separately for GOOD and BAD), and entered

365 into group-level analysis. At the group level, we identified those regions that exhibited both i)
 366 increasing activation with increasing updates in GOOD trials, as well as ii) increasing
 367 activation with decreasing updates in BAD trials, specified by the difference contrast
 368 ($PM_update_{GOOD} > PM_update_{BAD}$). In addition, we reported global conjunction results to
 369 clarify whether the difference related to different magnitudes of the same modulation effect
 370 (e.g., the positive correlation between BOLD and update was stronger in GOOD than in
 371 BAD), or to modulation effects of opposite direction (e.g., the correlation between BOLD and
 372 update was positive in GOOD, but negative in BAD). Moreover, we tested whether the
 373 magnitude of the favorable updating effect correlated with the optimism bias across subjects
 374 by conducting a covariate analysis with one contrast per subject ($PM_update_{GOOD} >$
 375 PM_update_{BAD}).

376 Finally, we conducted two additional GLMs with categorical designs that split all
 377 trials into three sizes of update (small, mid, and large), separately for GOOD and BAD. To
 378 approximate the adjustment for EE within the modulation by update, we subtracted EE from
 379 update at each trial ($update' = update - EE$). That way, we controlled for the general effect
 380 that updates tend to be larger after larger EE, which may confound with the valence effect.
 381 Note that dividing update by EE would not be optimal because all trials with an update equal
 382 zero ($M = 30.09\%$, $SD = 16.13$) would have yielded zero as well, irrespective of EE. This
 383 would not be appropriate because meaningful differences between zero updates in response to
 384 EEs of different sizes (e.g., $EE = 2$ and $EE = 20$) would have been concealed. For each
 385 subject, the numbers of trials across the three categories of updates were kept as similar as
 386 possible (numbers of trials did not differ; GOOD: $M = 13.32$, $SD = 0.85$, $F(2,69) = 0.58$, $p =$
 387 $.560$; BAD: $M = 12.74$, $SD = 1.02$, $F(2,69) = 0.09$, $p = .913$).

388 First, we used a GLM that modeled the three categories of update sizes separately for
 389 GOOD and BAD (six regressors) in order to be able to illustrate group effects of different
 390 sizes of updates on the BOLD signal (**Figure 3B**, line chart). Second, we used another

391 categorical GLM as a basis for the DCM analysis because the categorical levels can be more
 392 easily interpreted as inducing contextual modulatory effects in DCM than parametric
 393 variables (Stephan et al., 2010). According to the valence of updating schematically shown in
 394 **Figure 3B** (gray box), this GLM collapsed the different update sizes into three valence
 395 categories corresponding to *unfavorable* (small_{GOOD} and large_{BAD} updates, U), *mid* (mid
 396 updates, M) and *favorable* (large_{GOOD} and small_{BAD} updates, F) updating (**Figure 3C**). Three
 397 contrast images were computed relative to the implicit baseline ($E2_{\text{unfavorable}}$, $E2_{\text{mid}}$ and
 398 $E2_{\text{favorable}}$), and entered into group-level analysis. At the group level, we tested for brain
 399 regions that exhibited greater activation for favorable updates than for unfavorable updates
 400 ($E2_{\text{favorable}} > E2_{\text{unfavorable}}$). In addition, we identified those regions that were activated during
 401 updating independent of the valence (i.e., conjunction of all three levels of E2).

402

403 *DCM Analyses*

404

405 DCM represents a hypothesis-led approach to understand neural circuits underlying
 406 observed brain responses (Friston, 2011). We used DCM to estimate and infer causal
 407 interactions among brain regions involved in belief updating (i.e., during the E2 event). To
 408 this end, competing models with different intrinsic coupling between regions, and different
 409 task-dependent modulations of these couplings, were specified. Each model corresponded to a
 410 specific hypothesis about how observed data were caused, and Bayesian model selection was
 411 used to quantify the evidence for one model over another (Friston, 2011). Model inversion
 412 provided estimates of the model evidence and the corresponding effective connectivity. We
 413 tested whether the context of favorable and unfavorable updating modulated the coupling
 414 between distributed brain responses, and whether value-coding regions exerted influence on
 415 other regions associated with cognitive processing.

416 First, we selected the nodes for the DCM based on the group results revealed by the
417 simplified categorical GLM with three categories of valence of updates (unfavorable, mid and
418 favorable). The time series were extracted by computing the principal eigenvariate from 4 mm
419 diameter spheres (33 voxels) centered on the peak coordinates and adjusted for the effect of
420 interest (F-contrast across the three categories of updates and the respective time derivatives).

421 Second, we specified competing models varying in their endogenous coupling and
422 valence-dependent modulatory effects and inverted each model for every subject. Given that
423 every brain region is connected reciprocally (Friston, 2011), the coupling in all models was
424 cyclic, i.e., all forward connections were accompanied by respective backward connections.
425 We used a random-effect Bayesian model comparison to infer the optimal model structure by
426 selecting the model with the best balance between accuracy and complexity.

427 Third, following the model selection, we performed a random-effect analysis of
428 parameter estimates derived from the selected model using one-sample t-tests (Stephan et al.,
429 2010). Additionally, we tested for correlations between parameter estimates and the optimism
430 bias. For the sake of completeness, we report correlations between the two bias measures
431 (optimism bias and Asymmetry) and all model parameters in **Table 4**. Bonferroni correction
432 was used to control for multiple comparisons: significance thresholds were adjusted for 7 tests
433 for the matrix A parameters ($p < .007$), and 2 tests for the expected correlations ($p < .025$).

Results

Task Performance

In the belief update task, subjects were asked to reconsider their risk estimates after being confronted with either good news (base rates of the risks were *lower* than initially expected), or bad news (base rates were *higher* than initially expected; **Figure 1**). In order to assess valence-biased belief updating, we first tested whether subjects were more likely to take into account good news (GOOD) rather than bad news (BAD). Indeed, belief updates (the difference between the self-related risk estimates before and after being presented with the actual base rate) following good news were significantly larger than the updates after bad news, $t(23) = 2.12$, $p = .045$, paired t-test, $d = 0.43$ (**Figure 2A**, see **Table 1** for the summary of all task variables). Furthermore, linear regression analyses revealed that updates were larger in GOOD than in BAD trials even after controlling for trial-wise estimation error (EE), $t(23) = 3.03$, $p = .006$, $d = 0.62$, or for estimated base rate (eBR), first self-related risk estimate (E1) and EE, $t(23) = 2.55$, $p = .018$, $d = 0.52$, one-sample t-tests. Thus, these results indicate that belief updates were optimistically biased.

In order to implement an even more precise control for potential confounds, and to further inform the fMRI analyses, we applied computational modeling. We tested whether the learning from actual base rates was asymmetric (different for GOOD and BAD, indicated by the parameter *Asymmetry*) while taking into account the EE, the personal relevance of the new information (PR), and the general tendency to learn from new information (learning rate component *Alpha*). Here, the EE was an important confound because larger errors generally tend to trigger larger updates. Also, when the new information is not regarded as personally relevant, updating of related beliefs tends to be reduced.

Bayesian model comparison of four competing models (αA , α , A , \emptyset) provided additional support for the optimism bias. It revealed that the ' αA '-model, that estimated both *Alpha* and its *Asymmetry* separately for each subject, predicted subjects' behavior significantly better than all other model versions (α , *Alpha* fitted, *Asymmetry* fixed to 0; A , *Alpha* fixed to 1, *Asymmetry* fitted; or \emptyset , *Alpha* fixed to 1 and *Asymmetry* fixed to 0), $E_f = .87$, $pxp = .994$ (**Figure 2B**). *Asymmetry* was significantly larger than zero, $M = 0.05$, $SD = 0.07$, $t(23) = 3.59$, $p = .002$, one-sample t-test, $d = 0.73$, showing that participants' learning rates were higher in response to good news than to bad news (LR_{GOOD}: $M = 0.79$, $SD = 0.19$, LR_{BAD}: $M = 0.70$, $SD = 0.18$; **Figure 2C**). Furthermore, *Alpha* was significantly smaller than 1, $M = 0.74$, $SD = 0.18$, $t(23) = -7.18$, $p < .001$, one-sample t-test, $d = 4.26$, showing that updates were on average smaller than the estimation errors. Finally, the optimism bias (derived from the observed task performance, mean update_{GOOD} – mean update_{BAD}) and the *Asymmetry* parameter (derived by the winning model ' αA ') were significantly correlated, $r = .79$, $p < .001$ (**Figure 2D**). While expected, the close relationship between these two bias measures also confirmed that the potential confounding variables (EE, PR) had no systematic influence in our task. Thus, we can rule out that "seemingly optimistic updating" was induced by a differential consideration of estimation errors due to varying personal relevance (Shah et al., 2016, p. 92). Quite the contrary, the optimism bias was even stronger after taking EE and PR into account. Thus, it is likely that earlier studies demonstrating the optimism bias, but lacking the enhanced experimental or formal computational control (Sharot et al., 2011; Sharot et al., 2012; Garrett et al., 2014; Korn et al., 2014; Kuzmanovic et al., 2015, 2016a; Kuzmanovic et al., 2016b), are also not affected by these potential confounds. Furthermore, correlations between the different task variables, computed separately for trials with good news and bad news and then averaged across subjects (**Figure 2E-F**), show that EE and updates correlated only very weakly with eBR, BR, E1, and E2 (\bar{r} s ranging from -.15 to .30). This is particularly important as it demonstrates that we succeeded in manipulating the

desirability of EE independently of prior beliefs (i.e., the size of risk estimates eBR and E1). Furthermore, it shows that the valence of updates was independent of the size of the estimated risks (eBR, E1) or the presented base rates (BR). Together, these findings provide a strong support for the notion that the difference in updating indeed reflected a valence-dependent consideration of the new information.

Moreover, we assessed the updates that were simulated by the winning model ‘ αA ’ assuming asymmetric learning rates, and by the unbiased model ‘ α ’, given the trial-by-trial PR and EE. The updates simulated by the model ‘ αA ’ corresponded well to the actually observed updates ($M_{\text{GOOD}} = 7.59$, $SD = 2.43$; $M_{\text{BAD}} = 6.49$, $SD = 2.09$, see white dots in **Figure 2A**) and were larger in GOOD than in BAD trials, $t(23) = 3.85$, $p = .001$, paired t-test, $d = 0.79$. In contrast, the updates simulated by the unbiased model ‘ α ’ did not differ across GOOD and BAD trial ($M_{\text{GOOD}} = 7.06$, $SD = 2.21$; $M_{\text{BAD}} = 7.02$, $SD = 2.20$, $t(23) = 0.22$, $p = .830$, paired t-test, $d = 0.04$; see gray dots in **Figure 2A**). This comparison proves that subjects’ asymmetric updating represents a true bias attributable to the different valence of the new information (good and bad news) and cannot be explained by any variations of other trial-by-trial variables (i.e., PR or EE; see Shah et al., 2016; Kuzmanovic and Rigoux, 2017).

Furthermore, we compared floor and ceiling effects across GOOD and BAD and showed that controlling for these effects even enhanced the optimism bias effect. Floor and ceiling effects could occur if the size of the possible update was limited by the response scale (probabilities from 1% to 99%). For example, in a GOOD trial, given an EE = 5 (e.g., eBR = 10%, BR = 5%) and an E1 = 3%, a subject would have only a limited space on the response scale to make an update toward a lower risk estimate (from E1 = 3% to the end of the response scale of 1%). Critically, this possible update should be at least as large as the size of the estimation error in order to enable unconstrained updating. This is rather conservative because the general learning rate component *Alpha* was significantly smaller than 1 and because EE were also weighted by personal relevance that ranged between 0 and 1. In order to

test for floor and ceiling effects, we computed the size of possible update relative to EE for each trial ($\text{updspace-EE}_{\text{GOOD}} = (E1-1) - \text{EE}$; $\text{updspace-EE}_{\text{BAD}} = (99-E1) - \text{EE}$). Updspace-EE was lower in GOOD than in BAD, $t(23) = -4.50$, $p < .001$ ($M_{\text{GOOD}} = 28.24$, $SD = 11.03$; $M_{\text{BAD}} = 47.31$, $SD = 10.51$). Furthermore, the number of constrained update spaces ($\text{updspace-EE} < 0$) was higher in GOOD than in BAD, $t(23) = 5.08$, $p < .001$ ($M_{\text{GOOD}} = 6.17$, $SD = 5.45$; $M_{\text{BAD}} = 0.58$, $SD = 0.77$). Repeating the analyses after excluding the trials with a constrained update space revealed an even stronger optimism bias effect, $t(23) = 3.54$, $p = .002$, paired t-test, $d = 0.72$, $M_{\text{GOOD}} = 8.20$, $SD = 2.64$; $M_{\text{BAD}} = 6.80$, $SD = 2.23$, also when after controlling for trial-wise EE, $t(23) = 4.67$, $p < .001$, $d = 0.95$, or for eBR, E1 and EE, $t(23) = 4.10$, $p < .001$, $d = 0.84$, one-sample t-tests. Computational modeling analyses were not affected by the exclusion of trials with constrained updating due to formal consideration of the personal relevance: *Asymmetry* derived from the ‘ αA ’-model ($Ef = .86$, $pxp = .991$) was significantly larger than zero, $t(35) = 3.50$, $p = .002$, one-sample t-test, $d = 0.72$. Taken together, these tests show that the optimism bias effect was underestimated because of greater floor effects in GOOD trials.

We also examined the behavioral results after adding the 12 subjects with excessive motion to the sample of 24 subjects. These analyses yielded the same results as those with $n=24$. Belief updates following good news were significantly larger than the updates after bad news, $t(35) = 3.18$, $p = .003$, paired t-test, $d = 0.53$; *Asymmetry* was significantly larger than zero, $t(35) = 4.35$, $p < .001$, one-sample t-test, $d = 0.73$. Finally, the post-experimental debriefing revealed that none of the included subjects suspected that the purpose of the task was to assess difference in belief updating depending on the valence of the new information. At the end of the debriefing, we carefully explained the purpose of the study as well as the manipulation of the base rates in a standardized written form. Following this information, only one subject reported that he was aware of the good news-bad news effect during the own task performance. Furthermore, two subjects reported that they had no concerns with respect to the presented base rates during the task, the majority (17) reported that they were surprised

537 by some of the presented base rates but did not doubt their validity, five subjects doubted that
 538 single surprising base rates were really valid, and none of the included subjects reported
 539 having realized that the base rates were manipulated.

540

541 *fMRI Results*

542

543 *Error Tracking During BR.* Updating beliefs about self-related risks was triggered by
 544 erroneous expectations regarding the respective base rates. In order to investigate this crucial
 545 process, we identified brain regions that tracked the errors experienced upon the presentation
 546 of the actual base rates. The parametric modulation (PM) analysis revealed that error tracking
 547 recruited the anterior cingulate cortex (ACC), the inferior frontal gyrus (IFG), the anterior
 548 insula, the middle orbital gyrus and the dorsolateral prefrontal cortex (dlPFC; **Table 2**
 549 contrast 1b, and **Figure 3A**). In these regions, the activity increased with decreasing error size
 550 (negative correlation between BOLD and error) for both conditions GOOD and BAD (for an
 551 example, see the line chart in **Figure 3A** for the average activity in dlPFC across three sizes
 552 of error). This negative correlation seems unexpected because brain regions such as the ACC
 553 and the anterior insula have been associated with error processing, novelty, and task difficulty
 554 (Wessel et al., 2012; Klein et al., 2013; Shenhav et al., 2014; Kolling et al., 2016; Bastin et
 555 al., 2017; Fouragnan et al., 2017), and thus were expected to increase activity with increasing
 556 error size. However, a seminal study on belief updating has also demonstrated negative
 557 correlation between estimation error size and activity in the IFG, which was moreover
 558 predictive of trait optimism (Sharot et al., 2011). Thus, it may be necessary to reconsider the
 559 meaning of different outcomes in the specific context of the present experiment, because
 560 contexts determine the reference point for values of options (Palminteri et al., 2015).
 561 Subjects' task and their 'default option' was to revisit their prior beliefs due to new
 562 challenging information. Thus, in the majority of trials, subjects indeed were confronted with

base rates that markedly differed from what they expected and they updated their belief. Relative to this, encountering trials with a small error increases the difficulty of the decision whether to update beliefs (“Is the actual base rate different enough than expected, and is this difference relevant enough to drive an update of my own risk?”). Given the high accuracy of subjects’ base rate estimations in such trials, the alternative course of action to refrain from updating becomes increasingly valuable. We therefore speculate that increased activity in this network relates to enhanced initial comparison process that informs subsequent decisions about updating while maintaining behavioral flexibility (Kolling et al., 2016).

Furthermore, of all these error-tracking regions, only the activity in dlPFC correlated with the learning rate component *Alpha* (covariate analysis masked with the conjunction contrast PM_errorGOOD and PM_errorBAD, negative correlation; **Table 2** contrast 2). Betas indicating the strength of the linear relationship between error and BOLD were extracted for each subject (PM analysis, at the peak [40 38 30], averaged across PM_errorGOOD and PM_errorBAD), and plotted against *Alpha* for illustrative purposes (scatter plot in **Figure 3A**). Even when conducting the covariate analysis for the whole brain, an overlapping dlPFC cluster had the strongest correlation with *Alpha* (peak at [38 30 38], $T = 5.66$, 257 voxels), albeit at a more liberal significance threshold ($p < .05$, FWE-corrected at the cluster level).

The Valence of Updating. The main aim of the fMRI analysis was to identify brain regions that encoded the valence of updating. The valence of updating was defined based on how much the second estimation resulted in either favorable or unfavorable risk estimates, relative to the first estimation (see **Figure 3B**, gray box, for an illustration). Note that in GOOD trials, initial risk estimates were expected to *decrease* toward the actual base rate that was lower than expected. Conversely, in BAD trials, risk estimates were expected to *increase* toward the actual base rate that was higher than expected. In consequence, for GOOD trials, we assume that *large* updates would be experienced as *favorable*, because they result in lower

589 final risk estimates. In contrast, for BAD trials, we assume that *small* (or zero) updates would
 590 be experienced as *favorable*, because they prevent an increase of final risk estimates. Hence,
 591 we expected a *positive correlation* between the BOLD-signal and update in GOOD trials, and
 592 a *negative correlation* in BAD trials.

593 The parametric modulation analysis revealed that activity in the vmPFC had exactly
 594 this pattern (**Figure 3B** and **Table 3**, contrast 1a), indicating that this region tracked favorable
 595 updating. The correlation between the BOLD-signal in the vmPFC and update was greater in
 596 trials with good news than in trials with bad news (i.e., $PM_update_{GOOD} > PM_update_{BAD}$).
 597 The conjunction contrast (i.e., PM_update_{GOOD} , positive correlation & PM_update_{BAD} ,
 598 negative correlation) confirmed that this effect implied contrary modulation effects for GOOD
 599 and BAD (positive correlation in GOOD, and negative correlation in BAD; see the line chart
 600 in **Figure 3B**). Moreover, the vmPFC was also the only area in the whole brain, in which the
 601 magnitude of this valence-tracking effect correlated with the optimism bias (**Table 3**,
 602 contrasts 2a-b). This relationship to the task performance was illustrated by extracting betas
 603 indicating the strength of the differential linear relationship between update and BOLD for
 604 each subject (PM analysis, at the peak -6 50 -18, $PM_Error_{GOOD} > PM_Error_{BAD}$), and
 605 plotting them against optimism bias (**Figure 3B**, scatter plot).

606 Importantly, by including multiple orthogonalized parameters, we assessed variance
 607 that was uniquely explained by different update sizes, above and beyond the effects of other
 608 relevant computational components of belief updating such as EE and PR (Mumford et al.,
 609 2015). Moreover, the valence-tracking effect in the vmPFC was significant even when we
 610 controlled for task variables other than EE and PR. Repeating the parametric modulation
 611 analysis while including BR as an additional regressor (four orthogonalized regressors: BR,
 612 PR, EE, update, separately for GOOD and BAD) yielded the involvement of the same vmPFC
 613 clusters for the three contrasts indicating the valence effect (see Table 3, 1a including the
 614 conjunction and 2b; significance threshold as in the main analysis). In addition, including BR

615 and E2 (five orthogonalized regressors: E2, BR, PR, EE, update, separately for GOOD and
 616 BAD) also confirmed the valence-tracking effect in the vmPFC with respect to all three
 617 contrasts (albeit the contrast 2b at a less stringent significance threshold of $p < .001$,
 618 uncorrected, cluster size 216). Thus, in contrast to previous studies investigating the
 619 rewarding effect of favorable new information per se (in the context of updating self-
 620 evaluations; Korn et al., 2012), the valence effect related to the *relative improvement or*
 621 *worsening of initial beliefs*, but not to the valence of final beliefs (E2) or the new information
 622 (BR), or to other variables (PR, or EE).

623 Once we have demonstrated the effect of favorable updating while adjusting for BR,
 624 E2, EE and PR using parametric modulation, we repeated the analysis with a simplified
 625 categorical model. Discrete levels of valence (e.g., unfavorable or favorable) can then be used
 626 in the following DCM analysis to specify contextual effects that modulate the intrinsic
 627 coupling within the update circuit. According to the principle introduced above (and in the
 628 gray box in **Figure 3B**), we specified three valence levels (**Figure 3C**): *unfavorable* updating
 629 (U, small_{GOOD} and large_{BAD} updates), *mid* updating (M, mid updates) and *favorable* updating
 630 (F, large_{GOOD} and small_{BAD} updates). As a result, we concatenated the valence of updates
 631 across trials with good and bad news. The simplified categorical analysis revealed similar
 632 results as the PM analysis, demonstrating greater activity in the vmPFC for favorable than for
 633 unfavorable updates (**Figure 3C** and **Table 3**, contrast 3a). Moreover, the dmPFC showed a
 634 similar pattern of activity as the vmPFC. In addition, we tested for the conjunction effect
 635 across all three valence categories to identify brain regions that were generally activated
 636 during updating, independent of valence. General updating revealed widespread activations
 637 including occipital, parietal and frontal cortices (**Figure 3C** and **Table 3**, contrast 3c).

638
 639 *The Timing of Updating.* In order to explore whether the valence effect of updating did
 640 manifest already during the processing of BR, we repeated the parametric modulation analysis

641 (including PR, EE, and update), but defined the event BR instead of E2 as the unmodulated
 642 regressor. In this analysis, the contrast $PM_update_{GOOD} > PM_update_{BAD}$ did not yield any
 643 significant effect, even when using the vmPFC cluster as an inclusive mask at a less stringent
 644 significance level ($p < .001$, uncorrected). This indicates that the encoding of the valence of
 645 belief updating by the vmPFC indeed occurred during the period of update consideration and
 646 not already during the reception of the new information.

647 This contradicts classical reinforcement tasks where belief updating is expected to
 648 occur upon a relevant outcome (e.g., if I choose the green and not the red square and win
 649 money, I update the value of choosing the green square immediately). However, there is a
 650 substantial qualitative difference between classical reinforcement tasks and the present task.
 651 Estimations of base rates of life events in a population recruit declarative memory to retrieve
 652 general knowledge, and the feedback about the actual base rates indicates how accurate one
 653 was. Furthermore, estimating one's own risks of experiencing adverse events in the future
 654 represents a more complex cognitive process (including autobiographic and declarative
 655 memory) than deciding whether to choose a green or a red square in a gambling game. Thus,
 656 it is plausible that subjects focused on their degree of accuracy at the time point of feedback
 657 and subsequently focused on the meaning of this new information for their own risk estimate.

658 Several arguments additionally support this notion. First, we explicitly instructed the
 659 subjects to reconsider their risk estimates during the “update phase” (first two seconds of E2,
 660 before the response buttons were activated, see Figure 1). Second, there was no need to
 661 memorize estimated and actual base rates (or first self-risk estimates) until the update phase
 662 because all preceding values were visible on the screen at all times (see Figure 1). Third,
 663 during the debriefing, a majority of subjects spontaneously reported that they were pleased to
 664 see that they were often quite accurate in estimating the base rates. And forth, inspecting the
 665 encoding of estimation errors upon presenting the actual base rates (i.e., parametric
 666 modulation of actual base rate presentation by orthogonalized PR and EE) revealed that the

activity in the bilateral ventral striatum was higher the smaller the estimation errors were (the more accurate the subjects were), irrespective of their personal relevance or desirability (i.e., for both good news and bad news; left striatum [-12 14 -6], 68 voxel; right striatum [14 12 -6], 73 voxel; $p < .05$, FWE-corr. at the peak level for the whole brain). The ventral striatum plays a central role in encoding positive prediction errors (Chase et al., 2015). In the context of a task where subjects estimated base rates and were confronted with actual base rates that differed from their own estimates to a varying extent, greater accuracy corresponded to positive prediction error. Together with the debriefing self-reports, this finding supports the assumption that subjects focused on the degree of their accuracy during the presentation of base rates and thus were likely to reconsider their own risks subsequently, at a segregated time point.

DCM results

After identifying the vmPFC as the valuation area in the context of belief updating, we applied DCM to test competing hypotheses about its causal role within the update circuit. First, we selected three nodes for the DCM based on the update-related group results revealed by the simplified categorical analysis (**Figure 3C** and **Table 3**, contrasts 3a-c). The first node was the dlPFC. This region was involved both in general updating (conjunction across all update categories, **Figure 3C**), as well as in tracking errors in relevant prior beliefs (regarding BR) that was predictive of individual learning rates (**Figure 3A**). Thus, within the network activated by general updating, we chose the peak nearest to the learning rate-associated error tracking effect (MNI peak coordinate [44 42 26]). In order to further ensure that the chosen dlPFC peak was indeed specifically recruited by updating, we contrasted the three E2 categories with E1 (second versus first self-risk estimation). In a separate group-level analysis with four contrast images (E2_{unfavorable}, E2_{mid} and E2_{favorable}, E1) we identified those regions

693 that were more activated during updating beliefs about risks than during forming initial beliefs
 694 about risks (i.e., $E2_{\text{unfavorable}}$, $E2_{\text{mid}}$ and $E2_{\text{favorable}} > E1$, contrast [1 1 1 -3]). Note that $E1$ and
 695 $E2$ were otherwise comparable with respect to visual and motor requirements (see Figure 1).
 696 This additional analysis confirmed that the dlPFC was significantly activated during belief
 697 updating relative to initial belief formation ($p < .05$, FWE-corr. at the peak level for the whole
 698 brain). Importantly, the dlPFC cluster overlapped with both the general updating conjunction
 699 effect and the error tracking effect. Given that the dlPFC is a crucial part of the working
 700 memory system for transient storage and manipulation of information (Eriksson et al., 2015),
 701 this region represents a key candidate for maintaining integrative information processing
 702 generally necessary for belief updating. We therefore refer to the dlPFC as the valence-
 703 independent “update processing” node. The second node was the vmPFC (MNI peak
 704 coordinate [-2 46 -22]). Its activity was greater in response to favorable than unfavorable
 705 updates, and this valence-coding effect predicted the individual magnitudes of the optimism
 706 bias (**Figure 3B-C**), thus forming a “valuation” node. Finally, we defined the dmPFC as our
 707 third node (MNI peak coordinate [-16 44 40]). This region demonstrated a similar activity
 708 pattern as the vmPFC in the categorical GLM (**Figure 3C**), but, in contrast to vmPFC, it has
 709 been associated with cognitive processes such as social inferences and perspective taking, and
 710 less so with reward processing (Bzdok et al., 2013; de la Vega et al., 2016). Thus, we will
 711 tentatively refer to the dmPFC as the “cognitive” node.

712 This simple architecture comprising three nodes allowed us to compare different
 713 models that implied either valence-guided or non-valence-guided explanations for the
 714 observed brain responses. Valence-guided explanations would be favored if the vmPFC were
 715 the source of both i) the valence-dependent filtering of the general update-processing signal
 716 and ii) the subsequent influence on other prefrontal regions. Alternatively, non-valence-
 717 guided explanations would be supported if the vmPFC would i) receive a signal that is already
 718 modulated in a valence-dependent manner and ii) have no driving influence on other

719 prefrontal regions. Thus, adopting a hypothesis driven approach, we limited our model space
 720 to ten DCMs corresponding to these competing theories about the neural processing of belief
 721 updating (**Figure 4A**). Although we could in principle construct a higher number of possible
 722 models, including more models would mainly obfuscate our analysis as additional alternative
 723 models would not be realistic (e.g., disconnected nodes), or be prone to overfitting while
 724 unable to provide a conclusive answer to our research question (e.g., valence modulates all
 725 connections).

726 In all ten models, the event corresponding to the second risk estimation (E2, all three
 727 categories of updates) was specified as the exogenous input (**Figure 4A**). This input entered
 728 the dlPFC (matrix C in DCM) because this region showed increased activity during all
 729 categories of belief updating (see the line chart in **Figure 3C**). The models differed in their
 730 endogenous coupling (matrix A in DCM) such that *m1* to *m5* assumed a flow of neuronal
 731 states from dlPFC via vmPFC to dmPFC, while in models *m6* to *m10* the flow was from
 732 dlPFC via dmPFC to vmPFC. Given that we expected that the vmPFC would influence the
 733 dmPFC, models *m6* to *m10* represented null-hypotheses assuming the opposite course of
 734 influence. Furthermore, we systematically selected each of the possible coupling parameters
 735 to be the target of the valence-dependent modulation (matrix B in DCM; unfavorable
 736 updating, U or favorable updating, F). Given that we expected that favorable and unfavorable
 737 updating would differentially modulate the coupling in the network, *m5* and *m10* represented
 738 null-hypotheses assuming no modulation at all. More specifically, we hypothesized that
 739 valence encoding would manifest through filtering of the incoming signal by the vmPFC, and
 740 that the resulting differential valuation would further influence dmPFC, as formalized in *m1*.
 741 Alternatively, the valence-dependent modulation could have affected one of the other
 742 couplings (e.g., from dlPFC to dmPFC as formalized in *m6*). In these cases, the filtering of the
 743 incoming signal would not be attributed to vmPFC, and/or there would be no primary
 744 influence of the vmPFC on dmPFC. Notably, all models except of *m5* and *m10* were equally

745 complex but differed with respect to the flow of neuronal states and the coupling which was
 746 subject to contextual modulation, allowing for evidence-based hypothesis testing.

747 Bayesian model comparison confirmed that the model *m1* had the greatest evidence,
 748 above and beyond chance, $Ef = .77$, $pxp = .999$ (**Figure 4B**). The selected model assumed a
 749 cyclic signal flow from the dlPFC via vmPFC to dmPFC and a valence-dependent modulation
 750 of the coupling from dlPFC to vmPFC. The low evidence of models *without* modulations (*m5*
 751 and *m10*) indicates that the valence-dependent modulation of effective connectivity was
 752 indeed necessary to adequately predict subjects' network activity. Furthermore, of the eight
 753 models *with* modulations, *m1* still had a profoundly higher evidence than *m6* and other
 754 alternative models. This finding supports the hypothesis that the vmPFC filtered the incoming
 755 signal in a valence-dependent manner and influenced the dmPFC.

756 Third, we further inspected and analyzed the parameter estimates derived from the
 757 winning model *m1*. We hypothesized that the magnitude of valence-dependent modulation
 758 (the difference between F and U, F-U) of the dlPFC-vmPFC coupling would correlate with
 759 the optimism bias across subjects, because the stronger this modulation, the greater should be
 760 the response of the vmPFC to different valences of updating. Furthermore, we expected that
 761 the strength of the connection from vmPFC towards dmPFC would also correlate with the
 762 optimism bias, assuming that this coupling represents the influence of valuation on ongoing
 763 cognitive processing. Modulation parameters and coupling patterns in the context of favorable
 764 and unfavorable updating are reported in **Table 4** and plotted in **Figure 4C**. On average, the
 765 coupling from dlPFC to vmPFC decreased in the context of unfavorable updating relative to
 766 favorable updating. However, this difference did not reach significance due to the large
 767 variance of modulation estimates for U and F. It is of greater importance though that the
 768 valence-dependent modulation of the dlPFC-vmPFC coupling (the difference between F and
 769 U, F-U) correlated with the size of the optimism bias across subjects (**Figure 4D**). This
 770 relationship explains how the data observed in the fMRI analysis were caused. Subjects with a

771 greater optimism bias had a stronger valence-dependent filtering by vmPFC, resulting in an
772 increased BOLD response to favorable than unfavorable updating in vmPFC. Moreover, the
773 individual strength of the coupling from vmPFC to dmPFC also correlated with optimism bias
774 (both correlations corrected for multiple comparisons). Thus, the stronger the optimism bias,
775 the stronger was the influence of valuation on ongoing cognitive processing, mediated by the
776 coupling from vmPFC to dmPFC. In addition, the inspection of all possible correlation
777 coefficients (**Table 4**) revealed that the endogenous self-connection of the dmPFC inversely
778 correlated with the optimism bias (not corrected for multiple comparisons). Thus, the stronger
779 the optimism bias, the weaker was the self-inhibition of the dmPFC. Taken together, these
780 parameter estimates indicate a self-enhancing cyclic flow between vmPFC and dmPFC. In
781 subjects with high optimism bias, the vmPFC filtered the incoming information dependent on
782 valence. This differential signal was then forwarded to the dmPFC and there enhanced by the
783 reduced self-inhibition.

Discussion

The present study provides converging evidence that the value of desirable beliefs can influence ongoing cognitive processing. Participants demonstrated an optimism bias as they were more likely to update beliefs regarding their risks in response to good news than bad news (learning that base rates of the risks were *lower* versus *higher* than expected). This finding was also confirmed by computational modeling that formally controlled for valence-unrelated variables that influence updating (estimation error and personal relevance of the new information; Shah et al., 2016; Kuzmanovic and Rigoux, 2017). Given that we i) ruled out these alternative, valence-independent explanations, ii) manipulated the desirability of the new information independently of prior beliefs, and iii) demonstrated that the optimism bias was unrelated to the size of risk estimates or base rates, we conclude that information integration was indeed biased by the motivation to adopt the most favorable beliefs about one's future.

Furthermore, fMRI results showed that the vmPFC tracked the value of updating. In the context of good news, large updates toward lower risk estimates improve the ultimate risk perception, but after bad news, large updates toward higher risk estimates worsen the ultimate belief. In turn, small updates (small or no change in beliefs) also acquire opposing values in the context of good and bad news, respectively: While small updates after good news are unfavorable as they disregard the opportunity to improve risk estimates, small updates after bad news are favorable because they prevent worsening of risk estimates. The activity pattern in the vmPFC showed exactly this pattern: it increased with *increasing* updates toward lower risks (after good news), and with *decreasing* updates after bad news. Thus, not only improving beliefs, but also avoiding the worsening of beliefs triggered the vmPFC activity. Previous studies on optimism bias that included risk estimates for self and a similar other person already indicated a positive value of avoiding threatening belief updates by

810 disregarding undesirable new information. Here, particularly the decreased updating in self-
 811 related trials with bad news (relative to a comparably high amount of updating in self-related
 812 trials with good news and all other-related trials) was driving the optimism bias (Kuzmanovic
 813 et al., 2015, 2016a). Furthermore, research on context dependency of option values has shown
 814 that both gaining a reward (i.e., improving the current state, e.g., change from 1\$ to 2\$) and
 815 knowingly avoiding punishment (i.e., current state is unchanged, e.g., 1\$, but the possible
 816 loss, e.g., -1\$, is avoided) acquired a positive value and were tracked by the vmPFC
 817 (Palminteri et al., 2015). Lesion studies (Camille et al., 2011) and meta-analyses (Yarkoni et
 818 al., 2011; Diekhof et al., 2012; Levy and Glimcher, 2012; Bartra et al., 2013; Clithero and
 819 Rangel, 2014; Chase et al., 2015) have consistently shown that vmPFC was associated with
 820 valuation of rewards. In light of this literature, our results highlight that not only external
 821 rewards such as food or money, but also intrinsic rewards such as favorable beliefs, recruit the
 822 same valuation system. Moreover, the vmPFC was shown to automatically encode the value
 823 of objects (faces, houses, and paintings), independently of the explicit task instruction
 824 (Lebreton et al., 2009). In line with this automatic valuation and studies demonstrating
 825 unconscious motivational influences (Pessiglione et al., 2007), debriefing in our study
 826 revealed that subjects were unaware of their valence-dependent updating indicating that the
 827 valuation of belief updates need not require a voluntary process.

828 Extending previous work (Kuzmanovic et al., 2016a), the tracking of valence by
 829 vmPFC could be uniquely attributed to update sizes, above and beyond the influence of
 830 estimation errors, personal relevance of errors, actual base rates or final risk estimates. In
 831 other words, valence of updating depended on *improvement or worsening* of final beliefs
 832 *relative to* initial beliefs, irrespective of the beliefs or the new information per se. Moreover,
 833 we hypothesized that the valence-tracking effect in the vmPFC would be more pronounced in
 834 subjects with greater optimism bias, because belief formation should be biased by the desire
 835 to make favorable updates only if favorable updates also have a positive value. While

836 favorable future outlooks are likely to be experienced as pleasant, the sensitivity to the value
 837 of such prospects may differ among individuals, dependent on their current state or their
 838 personality. Indeed, subjects with a stronger optimism bias exhibited a greater valence-
 839 tracking effect in the vmPFC, confirming that the vmPFC activity is sensitive to the subjective
 840 value of stimuli (Grabenhorst and Rolls, 2011; Winecoff et al., 2013).

841 But what was the mechanism underlying this valence-dependent recruitment of the
 842 vmPFC that was able to influence ongoing belief formation? One possibility is that in the
 843 context of favorable (relative to unfavorable) updating, the vmPFC amplified incoming
 844 signals and further influenced other prefrontal regions. Alternatively, vmPFC may be
 845 influenced by other prefrontal regions, whose activity have already been modulated in a
 846 valence-dependent manner. We tested these competing hypotheses by comparing dynamic
 847 causal models comprising regions differentially recruited during favorable and unfavorable
 848 updating. The models consisted of three nodes with distinct functional signatures: the dlPFC
 849 represented an “update processing” node that received the exogenous input, the vmPFC was
 850 included as the “valuation” node, while the dmPFC represented a “cognitive” node. The
 851 dlPFC was a part of an extended network that was generally involved in updating (both
 852 favorable *and* unfavorable). The same region was also engaged in tracking errors in base rate
 853 estimates, while the strength of this tracking was predictive of individual learning rates. In
 854 contrast, both vmPFC and dmPFC showed greater activity for favorable than unfavorable
 855 updating. Having demonstrated that the vmPFC tracked the valence of belief updating in a
 856 strictly-controlled task-related manner, we use the label “cognitive” node for the dmPFC to
 857 distinguish it from the valuation-related vmPFC. While we cannot specify the exact kind of
 858 cognitive processing associated with the dmPFC recruitment, recent meta-analyses indicate
 859 clear functional dissociations with vmPFC being selectively associated with reward-related
 860 tasks, and dmPFC being preferentially involved in cognitive processes such as social
 861 inferences and perspective taking (Bzdok et al., 2013; de la Vega et al., 2016). In the context

862 of reconsidering one's own risk with respect to that of others, social inferences and
 863 perspective taking seem highly plausible, and their valence-guided use may provide the means
 864 of arriving at a particular, preferred conclusion (Kunda, 1990; Shepperd et al., 2002).

865 The Bayesian model comparison identified an optimum dynamic causal model, that
 866 had a reciprocal information flow from dlPFC via vmPFC to dmPFC, with a valence-
 867 dependent modulation of the coupling from dlPFC to vmPFC. This shows that particularly the
 868 vmPFC filtered the incoming signal in a valence-dependent manner and influenced the
 869 dmPFC accordingly. Importantly, both of these circuit features predicted individual
 870 magnitudes of the optimism bias. Subjects with a stronger optimism bias showed a greater
 871 increase in the dlPFC-vmPFC coupling during favorable (relative to unfavorable) updating.
 872 Moreover, biased belief updating was greater, the stronger the transmission of this valence-
 873 dependent signal from vmPFC to dmPFC was. Thus, the magnitude of the influence of
 874 valuation on ongoing cognitive processing, mediated by the coupling from vmPFC to dmPFC,
 875 predicted how much participants were biased towards more favorable updates. This finding
 876 complies with previous studies on functional connectivity, where the increase in connection
 877 between vmPFC ([3 51 -16]) and dmPFC ([-15 56 37]) predicted greater context-initiated
 878 reevaluation of choice options across subjects (Rudorf and Hare, 2014).

879 Previous studies on effective connectivity identified the vmPFC as a *target* of the
 880 directional influence of other regions. The coupling from hippocampus to vmPFC was
 881 increased when people chose better remembered options (Gluth et al., 2015). Furthermore, the
 882 coupling from dlPFC to vmPFC was increased during decisions to resist tempting short-term
 883 rewards and to choose greater, but delayed rewards instead, and this effect was predictive of
 884 between-subject differences in delay discounting (Hare et al., 2014). These and our findings
 885 share the general idea of dynamic reciprocal influences between the valuation system and
 886 other cognitive systems. However, our study is the first to show the opposite direction of

887 influence, namely the influence of the vmPFC on the dmPFC that mediates value-guided
888 belief formation.

889 In the resulting mechanistic model of belief formation, the valuation of ongoing
890 conclusions influences further cognitive processing, which in turn determines the final belief.
891 Thus, our results provide novel evidence for the notion that motivation to maximize pleasant
892 beliefs reinforces those cognitive processes that are most likely to yield favorable
893 perspectives. Leaving no possibility of reinterpretation of the observed effects in entirely
894 valence-independent terms, we substantially contribute to resolving the still persisting “hot
895 versus cold cognition” controversy (Kunda, 1990). As soon as we have a preference for one
896 conclusion over another, we may be in danger of automatically adjusting the knowledge we
897 recall and the inferential rules we apply in such a way as to support the preferred conclusion.
898 This bias in our reasoning has far-reaching implications for diverse decisions we make in our
899 everyday life, be it in a private or in professional contexts. While it can serve to protect from
900 discouraging and gloomy beliefs, it may also promote risk underestimations and
901 discriminating judgments.

902 **Author Contributions**

903 Conceptualization, Methodology, Software, Validation, Investigation, B.K.; Statistical

904 Analysis, B.K. and L.R.; Writing, B.K., L.R., and M.T.; Supervision, M.T.

References

- Andersson JLR, Skare S, Ashburner J (2003) How to correct susceptibility distortions in spin-echo echo-planar images: application to diffusion tensor imaging. *Neuroimage* 20:870-888.
- Bartra O, McGuire JT, Kable JW (2013) The valuation system: a coordinate-based meta-analysis of BOLD fMRI experiments examining neural correlates of subjective value. *Neuroimage* 76:412-427.
- Bastin J, Deman P, David O, Gueguen M, Benis D, Minotti L, Hoffman D, Combrisson E, Kujala J, Perrone-Bertolotti M, Kahane P, Lachaux JP, Jerbi K (2017) Direct Recordings from Human Anterior Insula Reveal its Leading Role within the Error-Monitoring Network. *Cereb Cortex* 27:1545-1557.
- Bzdok D, Langner R, Schilbach L, Engemann DA, Laird AR, Fox PT, Eickhoff SB (2013) Segregation of the human medial prefrontal cortex in social cognition. *Front Hum Neurosci* 7:232.
- Camille N, Griffiths CA, Vo K, Fellows LK, Kable JW (2011) Ventromedial frontal lobe damage disrupts value maximization in humans. *J Neurosci* 31:7527-7532.
- Chase HW, Kumar P, Eickhoff SB, Dombrovski AY (2015) Reinforcement learning models and their neural correlates: An activation likelihood estimation meta-analysis. *Cogn Affect Behav Neurosci* 15:435-459.
- Clithero JA, Rangel A (2014) Informatic parcellation of the network involved in the computation of subjective value. *Soc Cogn Affect Neurosci* 9:1289-1302.
- Cumming G (2014) The new statistics: why and how. *Psychol Sci* 25:7-29.
- Daunizeau J, Adam V, Rigoux L (2014) VBA: a probabilistic treatment of nonlinear models for neurobiological and behavioural data. *PLoS Comput Biol* 10:e1003441.

- 930 de la Vega A, Chang LJ, Banich MT, Wager TD, Yarkoni T (2016) Large-Scale Meta-
 931 Analysis of Human Medial Frontal Cortex Reveals Tripartite Functional Organization.
 932 Journal of Neuroscience 36:6553-6562.
- 933 Diekhof EK, Kaps L, Falkai P, Gruber O (2012) The role of the human ventral striatum and
 934 the medial orbitofrontal cortex in the representation of reward magnitude - an
 935 activation likelihood estimation meta-analysis of neuroimaging studies of passive
 936 reward expectancy and outcome processing. Neuropsychologia 50:1252-1266.
- 937 Eil D, Rao JM (2011) The Good News-Bad News Effect: Asymmetric Processing of
 938 Objective Information about Yourself. Am Econ J-Microecon 3:114-138.
- 939 Eriksson J, Vogel EK, Lansner A, Bergstrom F, Nyberg L (2015) Neurocognitive
 940 Architecture of Working Memory. Neuron 88:33-46.
- 941 Fouragnan E, Queirazza F, Retzler C, Mullinger KJ, Philiastides MG (2017) Spatiotemporal
 942 neural characterization of prediction error valence and surprise during reward learning
 943 in humans. Sci Rep 7:4762.
- 944 Friston KJ (2011) Functional and effective connectivity: a review. Brain Connect 1:13-36.
- 945 Garrett N, Sharot T, Faulkner P, Korn CW, Roiser JP, Dolan RJ (2014) Losing the rose tinted
 946 glasses: neural substrates of unbiased belief updating in depression. Front Hum
 947 Neurosci 8:639.
- 948 Gluth S, Sommer T, Rieskamp J, Buchel C (2015) Effective Connectivity between
 949 Hippocampus and Ventromedial Prefrontal Cortex Controls Preferential Choices from
 950 Memory. Neuron 86:1078-1090.
- 951 Grabenhorst F, Rolls ET (2011) Value, pleasure and choice in the ventral prefrontal cortex.
 952 Trends Cogn Sci 15:56-67.
- 953 Hare TA, Hakimi S, Rangel A (2014) Activity in dlPFC and its effective connectivity to
 954 vmPFC are associated with temporal discounting. Front Neurosci 8:50.

- 955 Hughes BL, Zaki J (2015) The neuroscience of motivated cognition. *Trends Cogn Sci* 19:62-
956 64.
- 957 Klein TA, Ullsperger M, Danielmeier C (2013) Error awareness and the insula: links to
958 neurological and psychiatric diseases. *Front Hum Neurosci* 7:14.
- 959 Kolling N, Behrens T, Wittmann MK, Rushworth M (2016) Multiple signals in anterior
960 cingulate cortex. *Curr Opin Neurobiol* 37:36-43.
- 961 Korn CW, Prehn K, Park SQ, Walter H, Heekeren HR (2012) Positively biased processing of
962 self-relevant social feedback. *J Neurosci* 32:16832-16844.
- 963 Korn CW, Sharot T, Walter H, Heekeren HR, Dolan RJ (2014) Depression is related to an
964 absence of optimistically biased belief updating about future life events. *Psychological*
965 *Medicine* 44:579-592.
- 966 Kunda Z (1990) The case for motivated reasoning. *Psychol Bull* 108:480-498.
- 967 Kuzmanovic B, Rigoux L (2017) Valence-Dependent Belief Updating: Computational
968 Validation. *Front Psychol* 8:1087.
- 969 Kuzmanovic B, Jefferson A, Vogeley K (2015) Self-specific optimism bias in belief updating
970 is associated with high trait optimism. *Journal of Behavioral Decision Making*
971 28:281–293.
- 972 Kuzmanovic B, Jefferson A, Vogeley K (2016a) The role of the neural reward circuitry in
973 self-referential optimistic belief updates. *Neuroimage* 133:151-162.
- 974 Kuzmanovic B, Rigoux L, Vogeley K (2016b) Brief Report: Reduced Optimism Bias in Self-
975 Referential Belief Updating in High-Functioning Autism. *J Autism Dev Disord*.
- 976 Lebreton M, Jorge S, Michel V, Thirion B, Pessiglione M (2009) An automatic valuation
977 system in the human brain: evidence from functional neuroimaging. *Neuron* 64:431-
978 439.

- 979 Lefebvre G, Lebreton M, Meyniel F, Bourgeois-Gironde S, Palminteri S (2017) Behavioural
 980 and neural characterization of optimistic reinforcement learning. *Nature Human*
 981 *Behaviour* 1.
- 982 Levy DJ, Glimcher PW (2012) The root of all value: a neural common currency for choice.
 983 *Curr Opin Neurobiol* 22:1027-1038.
- 984 Mumford JA, Poline JB, Poldrack RA (2015) Orthogonalization of regressors in fMRI
 985 models. *PLoS One* 10:e0126255.
- 986 Palminteri S, Khamassi M, Joffily M, Coricelli G (2015) Contextual modulation of value
 987 signals in reward and punishment learning. *Nat Commun* 6:8096.
- 988 Palminteri S, Lefebvre G, Kilford EJ, Blakemore S-J (2016) Confirmation bias in human
 989 reinforcement learning: evidence from counterfactual feedback processing. In.
 990 *bioRxiv*, not peer-reviewed preprint.
- 991 Penny WD (2012) Comparing Dynamic Causal Models using AIC, BIC and Free Energy.
 992 *Neuroimage* 59:319-330.
- 993 Pessiglione M, Schmidt L, Draganski B, Kalisch R, Lau H, Dolan RJ, Frith CD (2007) How
 994 the brain translates money into force: A neuroimaging study of subliminal motivation.
 995 *Science* 316:904-906.
- 996 Power JD, Barnes KA, Snyder AZ, Schlaggar BL, Petersen SE (2012) Spurious but
 997 systematic correlations in functional connectivity MRI networks arise from subject
 998 motion. *Neuroimage* 59:2142-2154.
- 999 Rigoux L, Stephan KE, Friston KJ, Daunizeau J (2014) Bayesian model selection for group
 1000 studies - revisited. *Neuroimage* 84:971-985.
- 1001 Roese NJ, Olson JM (2007) Better, Stronger, Faster Self-Serving Judgment, Affect
 1002 Regulation, and the Optimal Vigilance Hypothesis. *Perspectives on Psychological*
 1003 *Science* 2:124-141.

- 1004 Rudman LA, Dohn MC, Fairchild K (2007) Implicit self-esteem compensation: Automatic
1005 threat defense. *Journal of Personality and Social Psychology* 93:798-813.
- 1006 Rudolf S, Hare TA (2014) Interactions between Dorsolateral and Ventromedial Prefrontal
1007 Cortex Underlie Context-Dependent Stimulus Valuation in Goal-Directed Choice.
1008 *Journal of Neuroscience* 34:15988-15996.
- 1009 Shah P, Harris AJL, Bird G, Catmur C, Hahn U (2016) A pessimistic view of optimistic belief
1010 updating. *Cognitive Psychology* 90:71-127.
- 1011 Sharot T, Garrett N (2016a) Forming Beliefs: Why Valence Matters. *Trends Cogn Sci* 20:25-
1012 33.
- 1013 Sharot T, Garrett N (2016b) Optimistic Update Bias Holds Firm: Three Tests of Robustness
1014 Following Shah et al. *Consciousness and Cognition* 50:12-22.
- 1015 Sharot T, Korn CW, Dolan RJ (2011) How unrealistic optimism is maintained in the face of
1016 reality. *Nat Neurosci* 14:1475-1479.
- 1017 Sharot T, Guitart-Masip M, Korn CW, Chowdhury R, Dolan RJ (2012) How dopamine
1018 enhances an optimism bias in humans. *Curr Biol* 22:1477-1481.
- 1019 Shenhav A, Straccia MA, Cohen JD, Botvinick MM (2014) Anterior cingulate engagement in
1020 a foraging context reflects choice difficulty, not foraging value. *Nat Neurosci* 17:1249-
1021 1254.
- 1022 Shepperd JA, Carroll P, Grace J, Terry M (2002) Exploring the causes of comparative
1023 optimism. *Psychologica Belgica* 42:65-98.
- 1024 Smith SM, Jenkinson M, Woolrich MW, Beckmann CF, Behrens TE, Johansen-Berg H,
1025 Bannister PR, De Luca M, Drobnjak I, Flitney DE, Niazy RK, Saunders J, Vickers J,
1026 Zhang Y, De Stefano N, Brady JM, Matthews PM (2004) Advances in functional and
1027 structural MR image analysis and implementation as FSL. *Neuroimage* 23 Suppl
1028 1:S208-219.

- 1029 Stephan KE, Penny WD, Moran RJ, den Ouden HE, Daunizeau J, Friston KJ (2010) Ten
 1030 simple rules for dynamic causal modeling. *Neuroimage* 49:3099-3109.
- 1031 Tesser A (2000) On the confluence of self-esteem maintenance mechanisms. *Personality and*
 1032 *Social Psychology Review* 4:290-299.
- 1033 Wessel JR, Danielmeier C, Morton JB, Ullsperger M (2012) Surprise and error: common
 1034 neuronal architecture for the processing of errors and novelty. *J Neurosci* 32:7528-
 1035 7537.
- 1036 Winecoff A, Clithero JA, Carter RM, Bergman SR, Wang L, Huettel SA (2013) Ventromedial
 1037 prefrontal cortex encodes emotional value. *J Neurosci* 33:11032-11039.
- 1038 Xu JQ, Moeller S, Auerbach EJ, Strupp J, Smith SM, Feinberg DA, Yacoub E, Ugurbil K
 1039 (2013) Evaluation of slice accelerations using multiband echo planar imaging at 3 T.
 1040 *Neuroimage* 83:991-1001.
- 1041 Yarkoni T, Poldrack RA, Nichols TE, Van Essen DC, Wager TD (2011) Large-scale
 1042 automated synthesis of human functional neuroimaging data. *Nat Methods* 8:665-670.
 1043

1044 **Figures and Figure Legends**

1045

1046 **Figure 1.** Outline and examples of experimental trials.

1047 The figure illustrates the outline of experimental trials, including hypothetical trial examples.

1048 Each experimental trial consisted of four succeeding events: With respect to a specific adverse

1049 life event (e.g., cancer), subjects had to estimate the base rate (eBR) and their own risk (E1).

1050 They were then presented with the actual base rate (BR) and had the opportunity to estimate

1051 their own risk again (E2). After identical eBR and E1, the upper progression of the trial exam-

1052 ple shows a BR *lower* than expected indicating good news, while the lower progression shows

1053 a BR *higher* than expected indicating good news. Estimation errors (EE) corresponded to the

1054 difference between the estimated and the actual base rate, and the update corresponded to the

1055 difference between the first and the second self-risk estimate. Note that in both trial examples,

1056 the EE is 10 and the update is 8. For eBR, E1 and E2, subjects were instructed to use response

1057 buttons to adjust the displayed number to match their estimate as soon as the number font

1058 changed to green (after 2 seconds). Inter-stimulus intervals between eBR, E1, and E2, as well

1059 as inter-trial intervals after E2, were jittered and consisted of a fixation cross (not shown

1060 here).

1061 **Figure 2.** Task performance and computational modeling.

1062 **A)** Bars show subjects' updates, that were significantly larger after good news (GOOD) than

1063 after bad news (BAD). White dots represent simulations of updates by the 'biased'

1064 computational model that assumes asymmetric learning rates for good and bad news (' αA ',

1065 two free parameters, *Alpha* and *Asymmetry*). Gray dots indicate simulated updates resulting

1066 from the 'unbiased' model that assumes identical learning rates for good and bad news (' α ',

1067 one free parameter, *Alpha*). The simulated unbiased updates provide a normative benchmark

1068 for rational updating with learning rates estimated for each subject under consideration of her

1069 or his exact trial history. Error bars show standard errors. **B)** Bayesian model comparison

1070 confirmed that the biased model ' αA ' best predicted subjects' updates. Model frequencies

1071 show that the majority of subjects was best described by the ' αA ' model, above and beyond

1072 chance (red dashed line). Error bars show the posterior variance. **C)** Learning rates extracted

1073 from the winning model αA were significantly higher after good than bad news. Error bars

1074 show standard errors. **D)** Optimism bias ($\text{update}_{\text{GOOD}} - \text{update}_{\text{BAD}}$) and *Asymmetry* (estimated

1075 for each subject by the model ' αA ') were significantly correlated (dots represent single

1076 subjects). **E-F)** Correlations between task variables separately for trials with good news (**E**)

1077 and those with bad news (**F**). * $p < .05$, **, $p < .01$.

Figure 3. Brain regions encoding errors and the valence of belief updating.

A) When being confronted with the actual base rate, errors in base rate estimation (weighted by the personal relevance) were tracked by the anterior cingulate cortex, the inferior frontal gyrus, the anterior insula, the middle orbital gyrus and the dorsolateral prefrontal cortex (dlPFC). The line chart shows that the activity in the dlPFC (representative of all clusters) increased with decreasing error size (parametric modulation by error, negative correlation). Of all the involved regions, only in the dlPFC did the magnitude of the error tracking correlated with the general learning rate component *Alpha* (see scatter plot). Thus, subjects with a stronger error tracking in the dlPFC also more strongly adjusted their initial beliefs in response to errors. **B)** During the second risk estimation, the activity in the ventromedial prefrontal cortex (vmPFC) encoded the valence of updating, adjusted for estimation error and personal relevance. The gray box schematically illustrates the opposed valences of increasing updates after good and bad news (in this example, eBR is equal to E1). After good news, large updates are favorable as they ultimately change beliefs toward lower risk estimates and small updates are unfavorable as they let the opportunity to improve risk estimates pass by. In contrast, after bad news, large updates are unfavorable as they ultimately change beliefs toward higher risk estimates and small updates are favorable because they prevent worsening of risk estimates. Resulting valences are summarized in the table below: unfavorable (U), mid (M) and favorable (F) updates. The line chart shows that the activity in the vmPFC tracked the positive valence as it increased with increasing update sizes after good news but decreased with increasing update sizes after bad news. The scatter plot shows that subjects with a greater tracking of favorable updating in the vmPFC were also more optimistically biased in their belief updating. **A-B):** The line charts and the scatter plots were not used for statistical inference (which was carried out in parametric modulation and covariate analyses within the SPM framework); they are shown solely for illustrative purposes. **C)** After demonstrating the valence effect with the more precise parametric modulation analysis presented in B), a

1104 simplified analysis of updating was conducted as a basis for DCM. Here, all trials were
1105 assigned to three valence categories: those with unfavorable (U), mid (M) and favorable (F)
1106 updates (adjusted for estimation error). Conjunction across these three categories revealed a
1107 distributed network involved in general updating, overlapping with the error tracking effect in
1108 the dlPFC. Comparing trials with favorable and unfavorable updates revealed the differential
1109 recruitment of the vmPFC and the dorsomedial prefrontal cortex (dmPFC) during updating.
1110 The line charts show contrast estimates in the dlPFC, vmPFC, and dmPFC, respectively.

1111 **Figure 4.** Neurocircuitry mechanisms underlying optimistic belief updating.

1112 **A)** Ten different dynamic causal models varying in intrinsic connectivity and contextual

1113 modulation (unfavorable and favorable updating, U and F) were specified. The model space

1114 encompassed three brain regions involved in updating: dorsolateral prefrontal cortex (dlPFC),

1115 ventromedial prefrontal cortex (vmPFC) and dorsomedial prefrontal cortex (dmPFC). **B)**

1116 Bayesian model selection revealed that the model *m1* best explained subjects' BOLD signal,

1117 above and beyond chance (red dashed line). In this model, the coupling between dlPFC and

1118 vmPFC was differentially modulated by unfavorable and favorable updating. Hence, the

1119 vmPFC filtered the incoming information in a valence-dependent manner, and furthermore

1120 influenced the dmPFC. **C)** Connectivity parameters derived from *m1* show that the coupling

1121 between dlPFC and vmPFC tended to be weaker in the context of unfavorable relative to

1122 favorable updating. **D)** Optimism bias correlated with two parameters of *m1* (highlighted in

1123 red): Differential modulation of the dlPFC-vmPFC connection by favorable vs. unfavorable

1124 updating (F-U), and the strength of the vmPFC-dmPFC connection (vmPFC::dmPFC). Thus,

1125 subjects with a stronger optimism bias also demonstrated a greater valence-dependent filtering

1126 of incoming information by vmPFC and a greater transmission of this differential signal

1127 further to dmPFC.

1128 **Tables**

1129

1130 **Table 1.** Task variables

Parameter	<i>M (SD)</i>		<i>p</i>	
	Good News	Bad News	Source	
Number of trials	39.96 (1.45)	38.21 (2.38)	.024	
Estimated base rate (eBR)	49.74 (12.67)	45.92 (12.30)	.000	<i>Participants' response</i>
First estimate (E1)	42.64 (11.10)	37.85 (10.49)	.000	<i>Participants' response</i>
Presented base rate (BR)	36.35 (12.57)	59.76 (12.22)	.000	<i>Base rate algorithm</i>
Estimation error (EE)	13.39 (0.95)	13.84 (0.57)	.001	$EE = eBR - BR $
Second estimate (E2)	35.12 (10.86)	44.55 (11.26)	.000	<i>Participants' response</i>
Update	7.51 (2.58)	6.70 (2.20)	.045	$Update_{GOOD} = E1 - E2,$ $Update_{BAD} = E2 - E1$
Personal relevance (PR)	0.70 (0.12)	0.69 (0.13)	.287	for $E1 < eBR$: $PR = 1 - ((eBR - E1) / (eBR - 1))$ for $E1 > eBR$: $PR = 1 - ((E1 - eBR) / (99 - eBR))$ for $E1 = eBR$: $PR = 1$
RT eBR (s)	5.19 (0.84)	5.11 (0.80)	.192	<i>Participants' response</i>
RT E1 (s)	3.25 (0.91)	3.30 (0.90)	.461	<i>Participants' response</i>
RT E2 (s)	2.70 (0.62)	2.56 (0.61)	.018	<i>Participants' response</i>

1131 *Note.* All measures (except for number of trials) were recorded or computed for each trial, and were then aver-
1132 aged, separately for the conditions GOOD and BAD, and separately for each participant. Positive update values
1133 indicated updates towards the BR, and negative values updates away from the BR (< 3% of the trials). PR: 1 in-
1134 dicates equal risk perception for the average and oneself; 0 indicates maximally different risk perception for the
1135 average and oneself; note that PR corresponds to 'relative personal knowledge' in Kuzmanovic et al., 2017. RT,
1136 reaction time. *p* values refer to paired two-tailed paired *t*-tests with $n = 24$.

1137 **Table 2.** Error coding during base rate presentation and its relation to the learning rate com-
 1138 ponent *Alpha*

	cluster		peak			
	size	<i>p</i> _{FWE-corr}		size	<i>p</i> _{FWE-corr}	
1) Parametric modulation of BR_{GOOD} and BR_{BAD} by error						
a) Conjunction: PM_error_{GOOD} & PM_error_{BAD}, positive correlation						
<i>No significant results</i>						
b) Conjunction: PM_error_{GOOD} & PM_error_{BAD}, negative correlation						
Anterior cingulate cortex	63	0	5.18	10	34	20
Inferior frontal gyrus (p. triangularis)	45	0.001	4.09	46	44	0
Anterior insula	37	0.001	4.05	28	22	6
Middle orbital gyrus	30	0.002	4	16	50	-2
dIPFC ^{COV_Alpha}	32	0.004	3.81	40	40	28
c) PM_error_{GOOD} > PM_error_{BAD}						
<i>No significant results</i>						
d) PM_error_{BAD} > PM_error_{GOOD}						
Cerebellum	48	0.001	6.9	-18	-76	-46
Middle occipital gyrus	83	0.005	6.17	-34	-84	28
Superior parietal lobule	47	0.006	6.15	24	-56	48
Conjunction: PM_error_{BAD}, positive correlation & PM_error_{GOOD}, negative correlation						
Inferior occipital gyrus	22	0.001	4.16	40	-84	-10
2) Covariate analysis of error coding with <i>Alpha</i> (masked with contrast 1b)						
dIPFC	12	.008	4.46	40	38	30

1139 *Note.* Error = EE * PR, based on the computational modeling of task performance. For significant differences
 1140 between PM_error_{GOOD} and PM_error_{BAD} we report global conjunction results to clarify whether the difference
 1141 relates to different magnitudes of the same modulation effect (e.g., the positive correlation between BOLD and
 1142 error was stronger in BAD than in GOOD), or to modulation effects of opposite direction (e.g., the correlation
 1143 between BOLD and error was positive in BAD, but negative in GOOD). ^{COV_Alpha} indicates that in this cluster the
 1144 magnitude of the error tracking correlated with the learning rate component *Alpha* across subjects (Covariate
 1145 analysis). dIPFC, dorsolateral Prefrontal cortex. Peak coordinates refer to the MNI space.

1146 **Table 3.** Activity during second estimation that was modulated by update

	cluster	peak				
	size	$p_{\text{FWE-corr}}$	T	x	y	z
1) Parametric modulation of E2_{GOOD} and E2_{BAD} by update						
a) PM_update_{GOOD} > PM_update_{BAD}						
vmPFC	49	0	5.63	-12	44	-16
		0.01	5.40	-6	44	-20
Conjunction: PM_update_{GOOD}, positive correlation & PM_update_{BAD}, negative correlation						
vmPFC	44	0	3.67	-8	46	-18
		0.02	3.35	-10	54	-12
b) PM_update_{BAD} > PM_update_{GOOD}						
<i>No significant results</i>						
c) Conjunction: PM_update_{GOOD} & PM_update_{BAD}, positive correlation						
<i>No significant results</i>						
d) Conjunction: PM_update_{GOOD} & PM_update_{BAD}, negative correlation						
Fusiform gyrus (V4)	816	0	7.33	28	-72	-8
Lingual gyrus (V1)		0	4.59	6	-72	2
Lingual gyrus (V3)	736	0	6.70	-10	-86	-6
Superior occipital gyrus (V3)		0	4.11	-16	-88	18
Superior occipital gyrus	231	0	5.17	22	-80	20
Precentral gyrus	494	0	4.54	-32	-18	64
Postcentral gyrus		0	4.34	-42	-26	54
Fusiform gyrus	25	0.01	3.53	24	-46	-14
2) Covariate analysis of valence coding with optimism bias						
a) Masked with contrast 1a, conjunction						
vmPFC	39	0	15.59	-6	50	-18
b) Whole brain						
vmPFC	14	.011	7.28	-2	48	-18
3) Three categories of E2: unfavorable, mid, favorable						
a) E2_{favorable} > E2_{unfavorable}						
vmPFC ^{DCM}	27	0	5.84	-2	46	-22
Dorsomedial prefrontal cortex	30	0.02	5.39	-16	44	40

b) E2_{unfavorable} > E2_{favorable}

No significant results

c) Conjunction: all 3 categories of E2

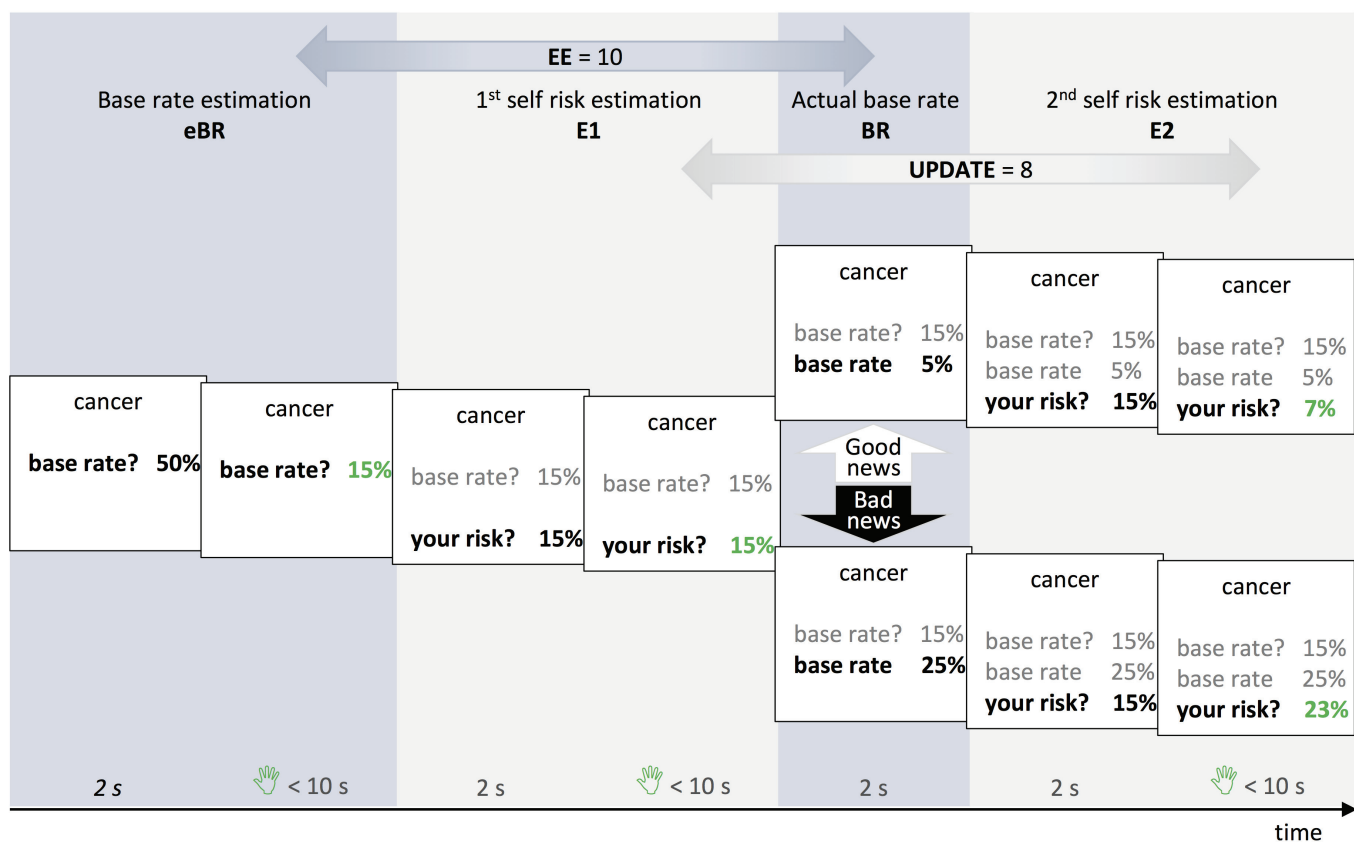
Lingual gyrus (V3)	57571	0	24	24	-86	-12
Fusiform gyrus		0	18.9	-30	-58	-14
Lingual gyrus (V4)		0	18.7	-24	-86	-14
Fusiform gyrus		0	16.4	32	-50	-18
Inferior parietal lobule		0	14.8	-44	-40	48
Inferior parietal lobule		0	12.6	50	-34	48
Thalamus		0	8.38	20	-30	-2
Middle frontal gyrus	6959	0	10.5	42	2	60
Inferior frontal gyrus (p. opercularis)		0	9.62	46	10	36
dIPFC ^{DCM}		0	8.99	44	42	26
dIPFC	1414	0	8.46	-28	52	28
dIPFC		0	8.21	-40	30	32
Inferior frontal gyrus (p.triangularis)		0	7.44	-34	34	24
Thalamus	136	0	6.58	-8	-22	8
Posterior cingulate cortex	125	0	6.13	-2	-24	28
Precentral gyrus	23	0.01	5.65	34	-28	72

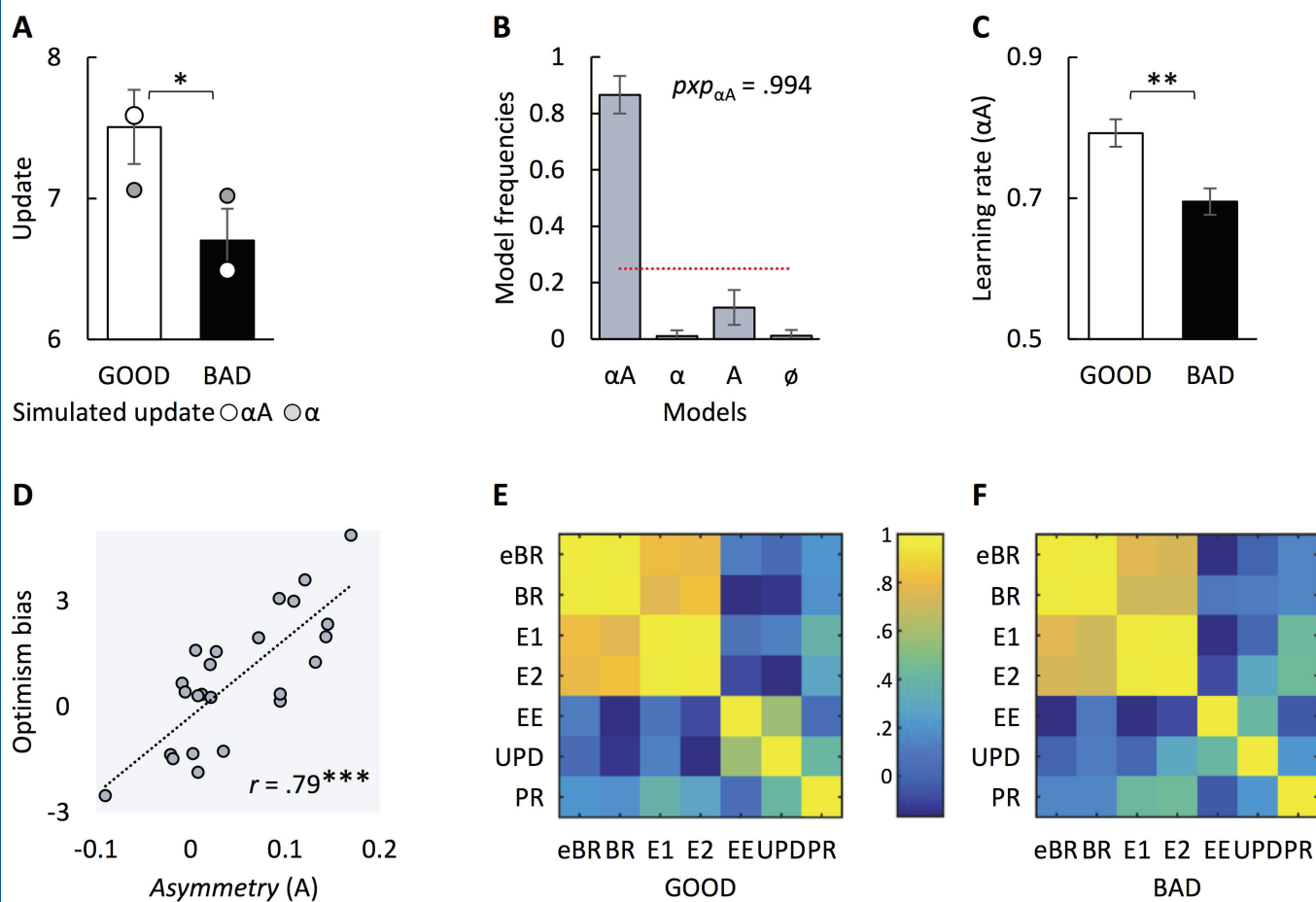
Note. For significant differences between PM_update_{GOOD} and PM_update_{BAD} we report global conjunction results to clarify whether the difference relates to different magnitudes of the same modulation effect (e.g., the positive correlation between BOLD and update was stronger in GOOD than in BAD), or to modulation effects of opposite direction (e.g., the correlation between BOLD and update was positive in GOOD, but negative in BAD). vmPFC, ventromedial prefrontal cortex; dIPFC, dorsolateral prefrontal cortex. Peak coordinates refer to the MNI space.

1153 **Table 4.** DCM parameter estimates of the model *m1* and correlations with measures of opti-
 1154 mism bias

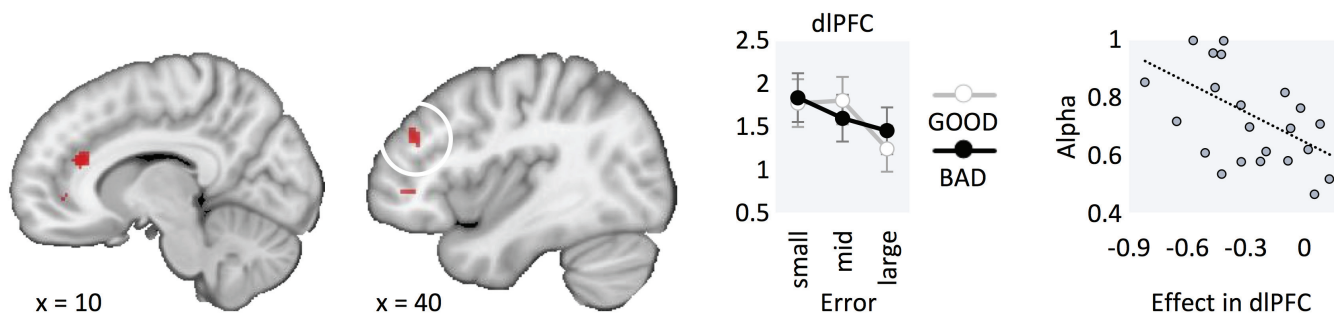
	<i>M (SD)</i>	<i>p</i> t-test	<i>r</i> Optimism bias	<i>p</i>	<i>r</i> Asymmetry	<i>p</i>
Matrix A						
dl::dl	-0.01 (0.09)	0.000*	-0.19	0.361	-0.21	0.323
dl::vm	-0.06 (0.12)	0.030	-0.23	0.277	-0.05	0.819
vm::dl	0.10 (0.15)	0.000*	-0.09	0.679	-0.15	0.485
vm::vm	-0.07 (0.09)	0.000*	-0.20	0.348	-0.20	0.342
vm::dm	0.15 (0.14)	0.000*	0.47	0.020*	0.49	0.015
dm::vm	0.08 (0.124)	0.004*	0.27	0.207	0.32	0.127
dm::dm	-0.02 (0.03)	0.001*	-0.49	0.015	-0.56	0.005
Matrix B						
U on dl::vm	-0.35 (1.06)	0.123	-0.23	0.275	-0.31	0.147
F on dl::vm	0.05 (1.00)	0.822	0.49	0.015	0.36	0.088
F - U	0.39 (1.42)	0.188	0.52	0.009*	0.48	0.018
Matrix C						
U M F to dl	0.12 (0.07)	0.000	0.20	0.340	0.13	0.541

1155 Notes. Parameter estimates in Hertz, self-connections were log-transformed. dl, dorsolateral prefrontal cortex;
 1156 vm, ventromedial prefrontal cortex; dm, dorsomedial prefrontal cortex; ::, endogenous connection; U, unfavora-
 1157 ble updating; M, mid updating; F, favorable updating. *, equivalent to $p < .05$, Bonferroni-corrected for multiple
 1158 comparisons (Matrix A, t-tests, $p < .007$ corrected for 7 comparisons; r , optimism bias, $p < .025$ corrected for 2
 1159 comparisons with a priori hypotheses).

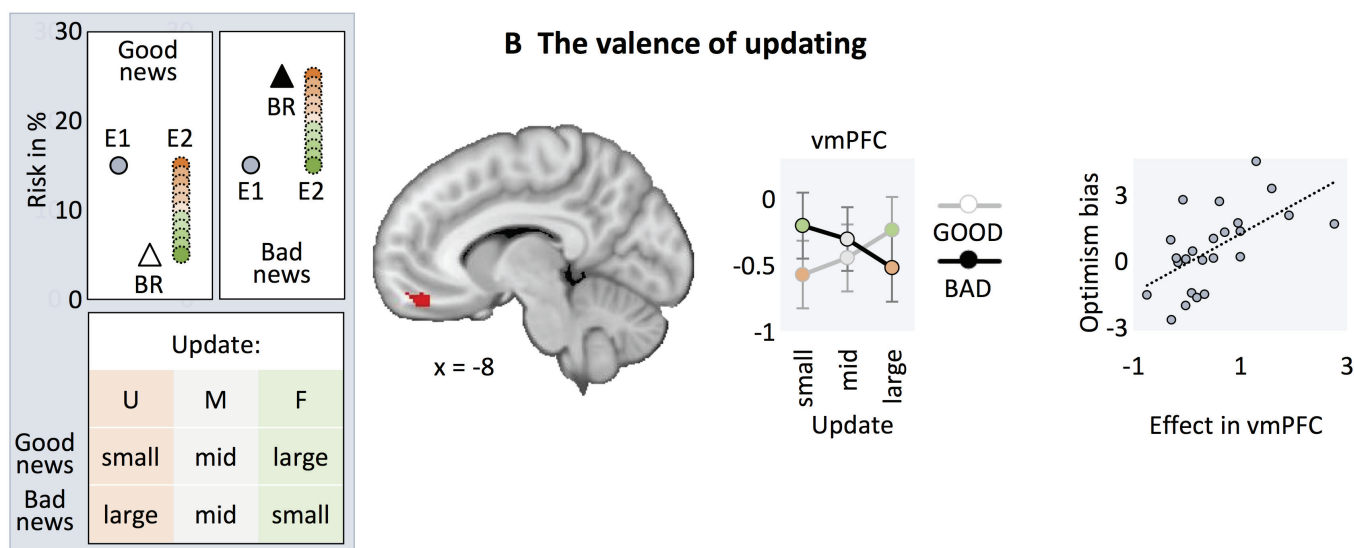




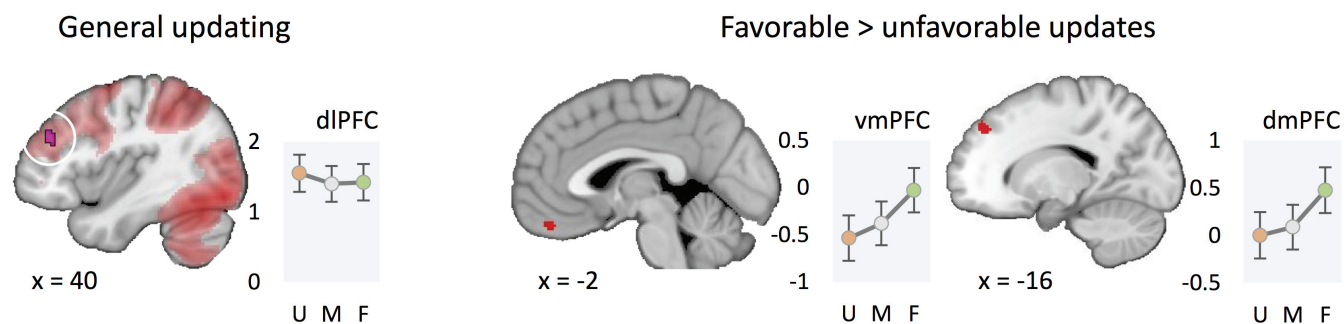
A Error tracking



B The valence of updating



C Three categories of updates



U, Unfavorable updates; F, Favorable updates; $p_{\text{FWE-corr.}} < .05$, peak level, whole brain; Error tracking effect

